2018-01-01

Design Of Robotic Tram Unit For Field Data Collection

Quetzalcoatl Mendoza Rosas
University of Texas at El Paso, qmendozaro@miners.utep.edu

DESIGN OF ROBOTIC TRAM UNIT FOR FIELD DATA COLLECTION

QUETZALCOATL MENDOZA ROSAS

Master's Program in Mechanical Engineering

APPROVED:

Louis Everett, Ph.D., P.E., Chair

Craig E. Tweedie, Ph.D.

Angel Flores-Abad, Ph.D.

Charles Ambler, Ph.D.
Dean of the Graduate School

Dedication

A mis padres, Rafael y Rosa, por su apoyo incondicional y sus enseñanzas a lo largo de mi vida, gracias por permitirme seguir mis sueños y haberme dado las herramientas para lograrlos. A mi hermana Ita, por su compañía y apoyo. Sin ustedes no hubiera podido logar esto.

A mi tío Jorge Espino y a mi tía Maribel Pimentel, sin ustedes ni siquiera hubiera soñado llegar tan lejos, gracias por su apoyo y motivación.

DESIGN OF ROBOTIC TRAM UNIT FOR FIELD DATA COLLECTION

by

QUETZALCOATL MENDOZA ROSAS, B.S.

THESIS

Presented to the Faculty of the Graduate School of

The University of Texas at El Paso

in Partial Fulfillment

of the Requirements

for the Degree of

MASTER OF SCIENCE

Department of Mechanical Engineering

THE UNIVERSITY OF TEXAS AT EL PASO

December 2018

Acknowledgements

First, I would like to express my sincere gratitude to Dr. Craig Tweedie and M.S. Gesuri Ramirez for allowing me to spend two fantastic years working at the lab, without your help this wouldn't be possible and to my advisor Dr. Louis Everett, thanks patience and guidance during my graduate studies.

Thanks to all my friends that walk alongside me on this part of my journey, Pablo, Arturo, Guillermo, Meny, Aaron, Gesuri, Motta and Tania, thanks for all your help and all the times spent together, wouldn't change it for a thing. And to my lab mates at the SEL, Roberto, Gesuri, Mauricio, Ari, Ale, and Hanggito. Thanks for your supports making and my days at the lab more enjoyable.

Abstract

Satellite remote sensing is the most applied method for detection and measurement of electromagnetic energy and its interaction with Earth surface. the analysis of the data acquired can provide important information with uses in areas as like weather forecasting, military intelligence and environmental and resources location. Due to the great distance from where the samples are taken and even with the most sophisticated sensor it is impossible to have an exactly replica of the Earth surface. As a result, scientist analyze imagery where a single pixel can be the representation of a 30 by 30 meters area of land. This could create misrepresentation of the properties, materials or distribution of the area of interest. As it is known, the veracity of a research depends on the reliability, precision and repeatability of sensors from which the data is collected.

"Mid-range" sensing is a short and long-term solution for spatial loss problem. This method measures the environment every few meters and generates several measure points that reciprocate a single pixel on a satellite measure allowing the description of the area of interest with more precision. This method is currently taken to the next stage by position more mid-range sensing station on different ecosystems and studying the relationships between their readings and the satellite images to create algorithms and model to approximate the spatial error and improve the data representativeness.

The main objective of this study is to analyze the current mid-range sensing system used by the System Ecology Lab at the University of Texas at El Paso, its working conditions and identify its limitation. This to prototype an autonomous robust tram unit that will be able to travel through the existing tramlines and to take reliable and relevant measurements that will allow development of new technologies and algorithms that will improve the remote sensing methods through image processing and mathematical models with low-budget investment in hardware.

The first stage consists in field tests of the current system, this would allow understand the functionality of the unit, its limitations, visualize improvement opportunities and analyze the working environment. Once the working conditions are defined a new design would be propose

and using engineering software simulations of strong winds loads, and instrumentation distribution will be prepared to calculate the center of mass and run a finite element and structural analyze on critical parts to validate the proposed prototype.

The analysis made to the cart structure along with the selection of materials ensures that this unit will perform correctly regardless the weather conditions. The prototype presented in this work have a stiffer, “weather-proof” structure and compartments that will improve the measurement taking at the JER site and allow it to have a permanent positioning on site. This improves the productivity of the research work by eliminating assembly/disassemble task. Thanks to the autonomy given to this unit, it could measure the field three times per week, increasing the previous number of measures taken with the old model and have the capability of running even when there is no one present at the site. By implementing simultaneous sensing with different sensor will open the doors for development of low-cost technology that through image processing will be able to obtain similar results that the ones obtain with expensive spectrometers.

Table of Contents

Acknowledgements v

Abstract vi

Table of Contents viii

List of Tables x

List of Figures xi

Chapter 1: Introduction 1

1.1 Remote Sensing 1

1.2 Remote Sensing Challenges 5

1.3 Literature Review 6

1.4 Thesis Motivation 7

Chapter 2: Problem 9

Chapter 3: Design 14

3.1 Technical specifications 14

3.2 New Design 17

Chapter 4: Structural Analysis 32

4.1 Structure definition 33

4.2 Loads definition 35

4.3 Calculations 36

Chapter 5: Finite Element Analysis 43

5.1 Model description 43

5.2 Mesh 45

5.3 Loads 46

5.4 Simulation 47

Chapter 6: Results 51

6.1 Final Model 51

6.2 Final Loads and Results 53

Chapter 7: Conclusions 67

7.1 Summary 67

7.2 Research Contributions 68
7.3 Future Work 69
References 70
Vita…. 71

List of Tables

Table 1.1. Electromagnetic spectrum region. 3

Table 3.1. Tram Cart new design specifications 17

Table 4.1 Tram carts components weight. 36

Table 4.2. Forces acting in each structural element. 38

Table 4.3 Spring's equations 41

Table 4.4 Rigid Body Equations 41

Table 4.5 Results 42

Table 5.1 Results comparison. 50

Table 6.1 List of materials. 52

Table 6.2. Resultant forces for top frame part. 54

Table 6.2 Forces influencing second system. 56

Table 6.3 Spring equations 57

Table 6.4 Rigid Body Equations 58

Table 6.5. Resultant forces for second system. 58

Table 6.6 Forces influencing tram cart. 60

Table 6.7 Tram cart's spring equations 62

Table 6.8 Tram cart's rigid Body Equations 62

Table 6.9. Resultant forces for tram cart. 62

Table 6.9. Resultant forces for tram cart with centered supports. 64

Table 6.10 Forces influencing tram cart. 65

Table 6.11 Resultant forces on tram cart supports. 66

Table 6.12 Resultant forces on tram cart centered supports. 66

List of Figures

Figure 1.1. Electromagnetic Spectrum. 1
Figure 1.2. Incident radiation – matter interaction. 2
Figure 1.3. Spectral Reflectance of different surfaces. 4
Figure 1.4. Reflected solar radiation on leaf. 5
Figure 2.1. SEL's site at Jornada Experimental Range 10
Figure 2.2.- Tram Cart current version. 10
Figure 2.3 Pictures taken by tram cart (comparison). 13
Figure 3.1 Aluminum profile used in Tram Cart. 18
Figure 3.2 Uniformly Distributed Load Cantilevered 18
Figure 3.3 Cart structure using T-Slots aluminum extrusions 19
Figure 3.4 Alternative designs 20
Figure 3.5 Tram unit drawings 21
Figure 3.6 Electronic components for data recollection 22
Figure 3.7 Top compartment 23
Figure 3.8 Door-like mechanism for Optic Fiber Sensors. 24
Figure 3.9 Side door mechanism for Optic Fiber Sensors. 25
Figure 3.10 Links, bottle and racked cap 25
Figure 3.11 Opening mechanism for optic fiber sensor 26
Figure 3.12 Supports for Optic Fiber Sensors. 26
Figure 3.13 a) base of top compartment. b) Components inside top compartment. 27
Figure 3.14 Bottom compartment 27
Figure 3.15. Tram unit structure 28
Figure 3.16 close up to anti-detach device 29
Figure 3.17 Charging ports first version. 29
Figure 3.18 Wheel-Plate charging port 30
Figure 3.19 Blade Charger. 31
Figure 4.1. Tram Cart Structure Design 32
Figure 4.2 Tie rods examples 33
Figure 4.3 Different supports for beam elements. 33
Figure. 4.4 Columns 34

Figure 4.5 beam elements at top of tram cart. 34
Figure 4.6 Structure elements. 35
Figure 4.7 Free Body Diagram of the structure. 37
Figure 4.8. Free Body Diagram simplified with forces and supports. 38
Figure 4.9 Top frame Free Body Diagram 39
Figure 5.1 a) Model; b) finite-element model 43
Figure 5.2 Tram Cart CAD assembly 44
Figure 5.3 Tram Cart simplify CAD 44
Figure 5.4 Default mesh generated by SolidWorks 45
Figure 5.5 a) Default Mesh; b) Refined Mesh using “Mesh Control”. 46
Figure 5.6 Final Mesh for structural analysis. 46
Figure 5.7. Pressure acting over top compartment. 47
Figure 5.8. Results of first simulation. 48
Figure 5.9 Final geometry with mesh, supports and loads. 48
Figure 5.10 Results of simulation a) stress in X direction; b) stresses in Z direction. 49
Figure 6.1. Screw and T-nuts used in joints 51
Figure 6.2 Fastener Applications. 51
Figure 6.3. Tram cart’s final design 52
Figure 6.4. Points of interest on top frame. 54
Figure 6.5 Manufacturer specification for corner gussets. 55
Figure 6.6. FBD of the second structure. 56
Figure 6.7. Tram cart’s FBD 59
Figure 6.8 a) cart with offset supports; b) cart with centered supports. 63
Figure 6.9 Tram Cart FBD, winds opposite direction. 64

Chapter 1: Introduction

1.1 Remote Sensing

Remote sensing can be simply defined as the collection of information about an object without making physical contact with it [1]. When talking about Remote Sensing of Environment (RSE) it is better to define it as the science of acquiring, processing and interpreting imaging and related data that record the interaction between matter (earth surface and atmosphere) and electromagnetic radiation. The interaction between matter and electromagnetic energy depends on the physical properties of the matter and the wavelength of electromagnetic energy that is used to sense. This being said, Remote Sensing of Environment can be referred to as the different methods that use electromagnetic energy to detect specific characteristics of a studied sample [2]. The remote sensing technics that many are familiar with started with the invention of photography in the first half of the nineteenth century and the implementation of aerial photography using balloons and kites capturing only data in the visible spectrum. Nowadays the most common methods use sensors mounted on satellites, spacecraft and planes and thanks to new technologies it is able to acquire data on multiple wavelength ranges, like ultraviolet (UV), infrared (IR) and microwave (Figure 1.1).

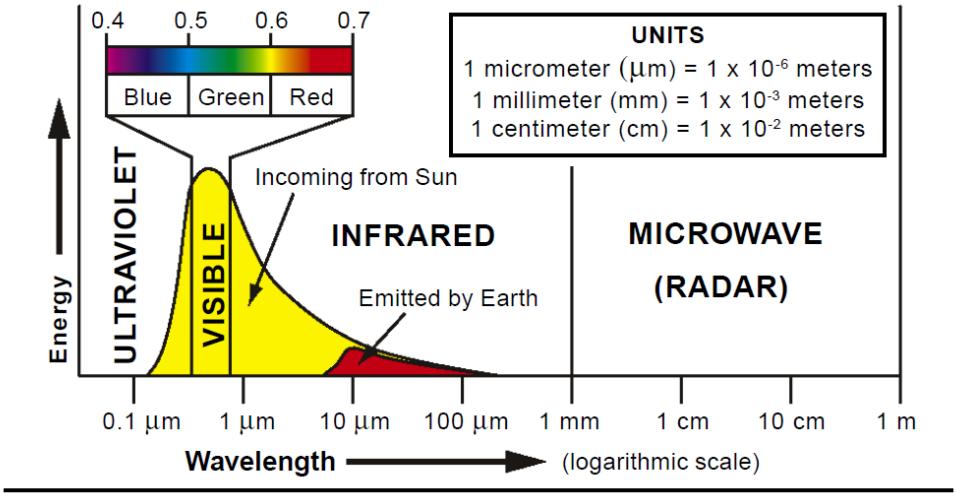

Figure 1.1. Electromagnetic Spectrum.

As described before, the remote sensing method measures the electromagnetic energy that comes in contact with matter, also known as incident radiation [2]. The interaction of these two can change certain properties of the incident radiation, principally its direction, intensity, wavelength and polarization. The figure 1.2 exemplifies four common outcomes of these interactions. All these interactions are record and interpreted to obtain the characteristics or the type of matter the electromagnetic energy encountered.

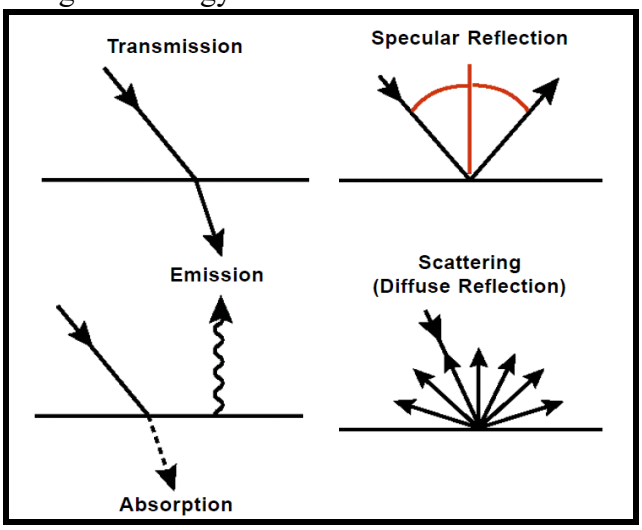

Figure 1.2. Incident radiation – matter interaction.

The earth's atmosphere composition allows it to absorb several wavelengths, decreasing the regions of the electromagnetic energy to measure. The regions absorb by the atmosphere are mainly the gamma-ray, X-ray and ultraviolet in part. Thus, the regions used in remote sensing of environment of earth are microwave, infrared, the visible spectrum and what is not absorbed from the ultraviolet. The Table 1.1 shows a more detail list of the electromagnetic spectrum regions and how they are affected by the earth's atmosphere [2].

Table 1.1. Electromagnetic spectrum region.

Region	Wavelength	Remarks
Gamma-Ray region	< 0.03 nm	Incoming radiation completely absorbed by the upper atmosphere and not available for remote sensing.
X-ray region	0.03 to 30 nm	Completely absorbed by atmosphere.
Ultraviolet region	0.03 to 0.3 μm	Incoming wavelength less than 0.3 μm completely absorbed by ozone in upper atmosphere.
Photographic UV Band	0.3 to 0.4 μm	Transmitted through the atmosphere. Detectable with film and photodetectors, but atmospheric scattering is severe.
Visible region	0.4 to 0.7 μm	Imaged with film and photodetectors. Includes reflected energy peak of earth at 0.5 μm.
Infrared region	0.7 to 100 μm	Interaction with matter varies with wavelength. Atmospheric transmission windows are separated by absorption bands.
Reflected IR band	0.7 to 3.0 μm	Reflected solar radiation that contains no information about thermal properties of materials. The interval from 0.7 to 0.9 μm is detectable with film and is called photographic IR band.
Thermal IR band	3 to 5 μm, 8 to 14 μm	Principal atmospheric windows in the thermal region. Images at these wavelengths are acquired by optical-mechanical scanners and special vidicon systems but not by film.
Microwave region	0.1 to 100 cm	Longer wavelengths that can penetrate clouds, fog, and rain. Images may be acquired in active or passive mode.
Radar	to 100 cm	Active form of microwave remote sensing. Radar images are acquired at various wavelength bands.
Radio	> 100 cm	Longest-wavelength portion of electromagnetic spectrum.

There are different systems for remote sensing and classifications, but the main one, just like most of the electronics devices and sensors, is passive and active. The passive systems detect naturally occurring radiation. These systems can be divided into, the ones that measure the radiation received from the sun (these work mostly with ultraviolet, near infrared and visible light radiation). And those that detect the thermal radiation emitted by all objects that are above absolute zero (works mostly in the infrared region of the electromagnetic spectrum) (Figure 1.1). The active

systems use its own source of radiation and measure what the surface of contact returns. Although these systems can basically use any type of electromagnetic radiation. The range of wavelength used is limited by the atmosphere and the effects it has over the different types of radiation. For these systems the observations mentioned before must be considered to be able to obtain representative data of the study objects.

The passive systems can be subdivided based on the sensors it uses. First there are the reflected solar radiation sensors, these measure the solar radiation reflected upward from surface features. Because these sensors depend on sun light they provide relevant data during daytime but can be affected by atmospheric conditions or changes in illumination during the day. Despite this, reflected solar sensing systems are the most used in remote sensing of environment. The second sub category are the Thermal infrared sensors. This type of sensor measures the thermal infrared radiation emitted by surfaces, revealing thermal properties of the surfaces. Because the temperature changes throughout the day the measurements taken by these sensors are linked to the time of the day when taken [3].

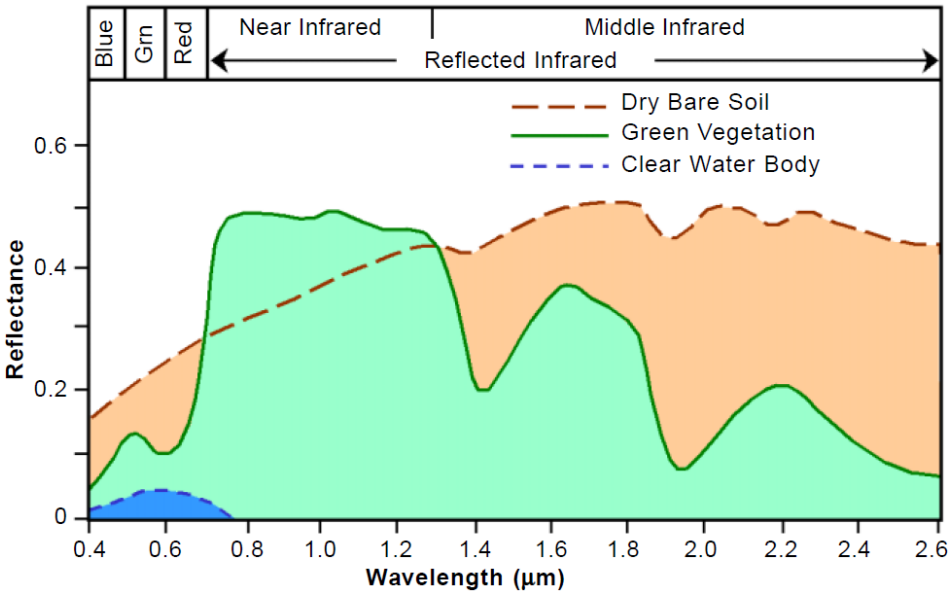

Figure 1.3. Spectral Reflectance of different surfaces.

Spectral signatures depend on the spectral reflectance of each kind of material (Figure 1.3), that is the ratio of reflected energy to incident energy as a function of wavelength [3]. The Spectral Signatures provide the key to discern different materials in images of reflected solar energy.

When monitoring specific surfaces, it provides information about its health, the most used method is the calculation of the Normalized Difference Vegetation Index (NDVI) that quantifies the vegetation "greenness", quality and growth by measuring the difference between near-infrared and red light (Figure 1.4). The NDVI range goes from +1 to -1, +1 been healthy vegetation, 0 no vegetation and <0 other type of surface, like water bodies among others, and can be calculated with equation 1.1 [3].

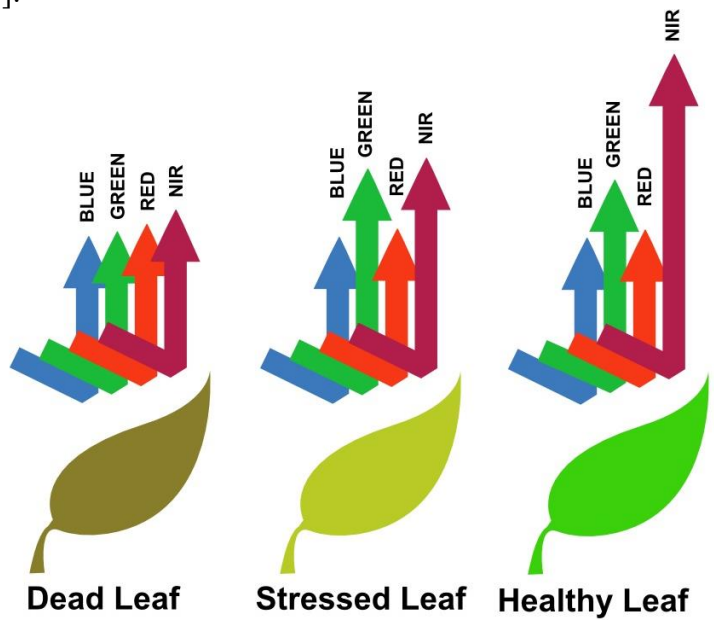

Figure 1.4. Reflected solar radiation on leaf.

$$NDVI = \frac{(NIR - R)}{(NIR + R)} \qquad eq.(1.1)$$

1.2 Remote Sensing Challenges

Satellite remote sensing is the most used method for detection and measurement of electromagnetic energy and its interaction with Earth's surface, and the analysis of the data acquired can provide important information with uses in areas like weather forecasting, military intelligence and environmental and resources location. Due to the great distance from where the

samples are taken and even with the most sophisticated sensor it is impossible to have an exact replica of the Earth's surface. Remote sensing provides imagery for a defined period or a discrete point in time, but with some loss of spatial resolution, depending upon the pixel size [4]. Flux towers (as Eddy covariance towers) may help with this problem, they can measure relatively small areas (a few hectares or less) but cannot readily isolate the contribution of component parts [5], they are limited to flat and uniform terrain, costly and cannot be installed in all sites.

Scientists have been looking into portable spectrometers for field measurements as a solution to this problem, but manual field measurements cannot sample in the same scale as satellite or tower-based systems, besides the human presence in the field can interfere with the tower measurements and disturb the ecosystem. Aircraft-based systems are an option, but they normally don't provide sufficient temporal coverage compared with the continuous flux sampling and their availability is limited. Therefore "mid-range" sensing systems started to be developed like the one used in this work.

1.3 Literature Review

"Mid-range" sensing systems have been used in the RSE area for a couple of years now. The model presented in this work is based on the one presented by John A. Gamon [5] which at the time was an adaptation of a track system developed at Oak Ridge, Tennessee [6]. This tram rail was placed near an eddy covariance tower and had a length of 100 m for regular and repeated sampling of the same areas for direct comparison. The cart had a dual-channel spectrometer for sensing radiation coming in both directions (from the sky and from the earth surface) and calculated the reflectance. Both sensors were fitted with fiber optics and mounted on the cart mast. The cart measures 12 by 24 by 18 inches with enough space to fit the spectrometers, data logger, computer and power supply, leaving enough space for adding a solar panel and more sensors in the future. It also counted with three operation modes, manual, semi-automatic and automatic [5].

The Mobile Instrumented Sensor Platform (MISP) is another system derived from the "Mid-range" sensing systems concept. This system was developed in part by members of the

Systems Ecology Lab (SEL) and is used in several locations across Alaska and Greenland. This system instead of using tracks is suspended directly above the areas of interest by stainless steel cables attach to two towers placed 50 meters apart each other. The MISP is equipped with infrared thermometers, net radiometers, NDVI sensors, sonic distance sensors and 3D video recorders. It has an aluminum frame that carries all the sensors, pulleys and motors to move across the transect. This system needs a 12-volt DC and a 115 volts AC power source, and it does not have a fully automated mode at the moment [6].

1.4 Thesis Motivation

The main objective of this work is to analyze the current working conditions of the tram cart and identify its limitation. Then to prototype an autonomous robust unit that will be able to travel through the existing track lines and to take reliable and relevant measurements that will allow development of new technologies and algorithms that will improve the remote sensing methods through image processing and mathematical models with low-budget investment in hardware.

The first stage consists of field tests of the current system, this would allow understanding the functionality of the unit, its limitations, visualize improvement opportunities and analyze the working environment. Once the working conditions are defined, a new design would be proposed and using engineering software simulations of strong loads and instrumentation distribution will be prepared to calculate the center of mass and run a finite element analyze on critical parts to validate the proposed prototype.

This work will conclude with the new design of a robotic tram unit for field data acquisition and will cover the selection of material and components, its distribution, validation of the design through computational simulation and the build of a prototype. Future works for adapting the unit for different working conditions will be open i.e. for the SEL site at Alaska or for other types of measurement.

The new system presented in this work will improve the measurement taking at the JER site and improve the productivity of the research work by eliminating this task from its list thanks to the autonomy given to this unit. It also will improve the quality of the data by taking more precise measurements and being able to run even when there is no one present at the site.

Chapter 2: Problem

The Systems Ecology Lab (SEL) is a multi-disciplinary laboratory that focuses on understanding the bio-complexity associated with environmental change and plant and ecosystem structure and function in extreme environments (namely Arctic tundra and the Chihuahua Desert). It uses a variety of plant ecological and physiological methods in combination with aerial and satellite remote sensing and Geographic Information Systems (GIS) to examine and model changes in plant and ecosystem structure and function over the range of spatial and temporal scales. The SEL is also committed to maintaining long-term environment observations and improving the capacity for cross-disciplinary and international cooperation in monitoring the impact of environmental change. This is done by developing novel internet-based portal, mapping and information management systems that facilitate access distributed information systems [7]. One of the main observation sites is located on the southwest of New Mexico state called Jornada Experimental Range and its run by collaboration of the University State and the USDA.

The Jornada Experimental Range (JER) was established in 1912 with the objective of widening recognition of, and concern about, rangeland degradation in the region and to demonstrate science-based solutions to this degradation. It has more than 200,000 acres of rangeland and all the research conducted here has led to important discoveries about ecosystems, from microscopic-scale studies of soil microorganisms to synoptic-scale assessments of vegetation patterns detected using satellite-based sensors [8].

The SEL's site at the Jornada Experimental Ranch (JER) is dedicated to monitor the changes in the rangeland, log them and make them available to the scientific community. It counts with a 110 meters long tram line for hyperspectral data collection, an Eddy Covariance tower, sensors network for monitoring changes in the environment, solar panels and power banks to supply energy to the sensors and the communication tower that provides the whole site with wireless internet connection (Figure 2.1). Once a week the Phenology Team goes to Jornada to collect data. They spend approximately four hours on the field, from 9 to past noon examining the

fauna, looking for changes from previous visits, the color of the leaves, the growth, the greenness, blooming and take notes about the weather conditions for these changes. At solar noon, the team starts working on the Tram cart to take the hyperspectral measurements. This process and the cart itself is explained in the next paragraph.

Figure 2.1. SEL's site at Jornada Experimental Range

Figure 2.2.- Tram Cart current version.

The current version of the Tram cart (Figure 2.2) consist in the next components: a wood compartment with aluminum reinforcements handles and wheels that carry the UniSpec-DC, a 12v battery, a mechanical trigger, the motor and a three-position switch for turning on and off the motor and changing direction. A two-piece arm with slots for an optic fiber sensor, Velcro to hold cables and sensors in place and a support for a digital camera (webcam). It is worth mentioning that this version must to be assembled before being operational and most of the electronic components are removed for better storage.

Before starting the measurements, there is a procedure to follow to get the tram cart ready. First take the cart body from its enclosure into the rails, once there, insert the two-piece arm into the slot on the side. These two parts make up the cart structure. For the electronics, first the battery and the Unispec-DC must be placed on the inside of the cart, once in, the battery is connected to the motor. After this the hyperspectral sensor that measures the reflectance is placed in the end of the arm into its slot, then carefully the optic fiber is taken into the inside of the cart without sharp turns and securing it with the Velcro. The same for the sensor that measures the light coming from the sun but on the other end of the arm. Both sensors are connected to the Unispec-DC in different channels. Finally, the webcam is inserted into its support and connected to an external laptop that is placed on top of the cart. That concludes the assembly of the cart but before running, it needs calibration and setting the trigger for the camera.

Lastly, it is needed to calibrate the hyperspectral reading unit. There are two calibrations, white calibrations and dark calibration. For the dark calibration the sensors are unplugged, and the terminals are covered with a black fabric to measure how much light is reflected by it. The same for white calibration, but this time using the sensors and a white standard. After calibration, a Bluetooth mouse is connected to act as a trigger for the camera and everything is ready to go.

The tramline is made of aluminum to avoid corrosion, it is 110 meters long and although the terrain is irregular, the tramline is completely straight with little change in elevation. Every meter the tramline has a special marking for the mechanical trigger to sense; this trigger is connected directly to the Unispec-DC and it then takes measurements with both sensors. This

allows the device to make automatic hyperspectral sensing. On the other hand, the RGB sensor has no shooting mechanism other than a Bluetooth mouse that needs to be operated by someone. Lastly, neither the cart nor the tramline has any form of protection for the cart against external forces trying to remove the cart from the line while operating.

To start the cart the operator needs to change the three-position switch from the middle position, the stop position, to either forward or backward according to the end he is at. When running, the cart can be stopped very easily, it goes slow so the operator just walks to it and changes the switch. While on the course the operator needs to be activating the camera shooter with the Bluetooth mouse, for this, he needs to walk alongside the cart across the track. One side of the tramline has been conditioned with a wooden trail, so the operator can move fluidly alongside the cart without disturbing the plants and terrain in its outskirts. Once the cart gets to the end of the rails, the operator recalibrates the hyperspectral sensors and changes position on the switch, so the cart can go back, this time measuring only with the hyperspectral sensors.

When the measurements are complete, the operator disassembles the cart, storing all its components safety and leaving the tramline empty. Then the field team take the laptop, the Unispec-DC and the battery back with them to the lab where they manually download and backup the data acquired and verify it for later upload to the servers. After that, the equipment is prepared for the next trip by charging them and deleting the previous data.

The areas of improvement can be divided into two. First the quality of the data, as mentioned in the previous paragraphs the collection of data depends to a certain extent on the user. Figure 2.3 shows four photos taken by the tram unit, these pictures were taken on different dates and are meant to be of the exact same area because they represent the same area taken by the hyper spectrometer. As mentioned, the hyper spectrometer or UniSpec-DC triggers automatically allowing it to measure the same area every time, while the RGB camera is controlled by the user, giving room for error and to capture an erroneous area.

Figure 2.3 Pictures taken by tram cart (comparison).

The second area of improvement is the hardware. As previously detailed, the tram unit has a functional but not very resistant build. Having materials like wood and Velcro strips that can be damaged or made unusable by weather conditions or misuse and they provide a weak protection to the electronic devices inside of it. By attacking these two areas the tram unit will have a better repeatability, become a more robust, durable and fully autonomous unit while providing the science community with higher quality data.

Chapter 3: Design

As mentioned in the previous section the current tram unit does its work, but it is very limited in functionality and its operation needs an operator most of the time while measuring. The purpose of this design will fix the problems with the current design improving not only the reliability of the data but also the productivity and relevance of the measurements, focusing in the working condition and using new technologies to create an efficient autonomous unit that could be activated remotely or automatically according to its schedule.

3.1 Technical specifications

The last section mentioned that the tram unit will need to withstand some extreme weather conditions while protecting all the electronic components. The Jornada's Experimental Ranch (JER) database was used to define the minimum conditions to withstand by the tram unit. This database helped quantify how much rain fell in the last 5 years along with the wind strength. This data provides maximum, minimum and the average to use as limitation. As mentioned before JER has a lot of different sites and with them different kind of sensors, this allows the administration to log all the information provided by the different sites and publish. All these logs can be accessed through their website [8]. The graph 3.1 compares the rain monthly average from 2015 against the long-term monthly average (1915-2015).

As for the weather conditions, the site is located on the desert section known as, the Chihuahua's desert and so it falls into the desert ecosystem category. This means it has extreme temperatures. During daytime, it may reach 50 °C, while in the night can go down to below zero. Deserts normally have less than 250 mm of rainfall per year, meaning that it is very scarce and unreliable [9]. According to the Jornada's database, the maximum temperature in the site is 60 °C. Most of the electronic components have a working temperate of up to 85 °C, so overheating will not represent a problem. For raining conditions, the heaviest rain was of 7.04 inches, for this we are using "weather-proof" compartments with an ingress protection of IPX4 [10].

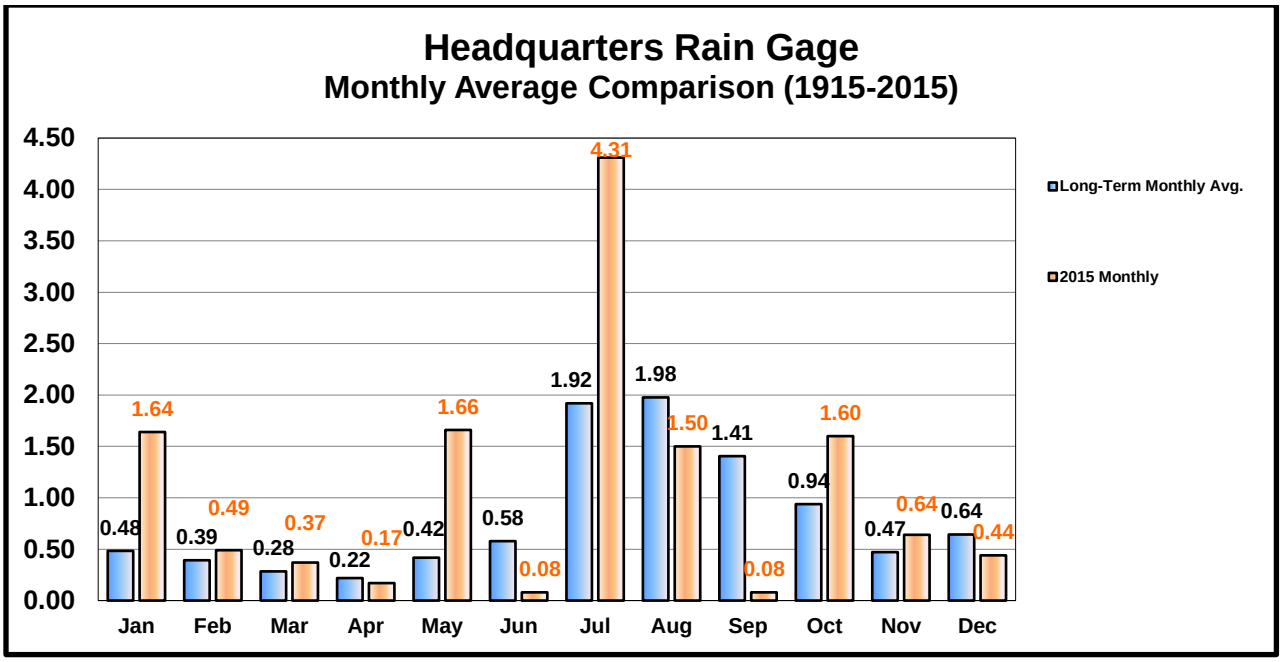

Graph 3.1 JER Headquarters Rain Gage Monthly Average Comparison (1915-2015)

Another issue to address are the loads that will be affecting the tram unit. In this particular case, there would be only two major loads in contact with the unit. The first will the distributive load equivalent to the wind. The Jornada's database gives an average of 17 meters per second and a mode of 20 m/s [8]. Based on that, the limit stablish will be the loads equivalent to winds of 20 meters per second. The other load to consider is its own weight. Because of the design, the overhanging arm and the components it will carry, will cause a moment that could turn over the tram unit and damage it. Also, there are big animals on Jornada, like cows and oryx, this will not represent a threat, this is because the site is fenced, and they cannot get in.

Because there are several components on the system and all of them need to communicate with each other is worth mention the stages of control and communication that the final system will have. There are seven stages overall. The first one uses the RS323 communications buss and it involves the control panel, the motor controller and the computer on the top. The motor controller connects directly to the motors and to the UniSpec-DC, this allows the other two to access the motors and the Hyper-spectrometer. On the top compartment are most of the sensors, these are connected directly to the computer using the I2C protocol. The cameras are also connected to that

computer through CSI protocol. Finally, there is a Serial port for debugging and a USB connection for a Wi-Fi antenna.

Component distribution helps to estimate the space required to store all the components and to visualize their positioning along with their interaction with its surroundings and have a better dimension estimation when buying or building the compartments. As described before, the tram unit will have two compartments, one at the bottom and one at the top. The bottom one will need to the have enough space for: the UniSpec-DC (25 x 15.5 x 8.5 cm), two 12 V batteries (15 x 9 x 6.5 cm), the RoboteQ AX1500 Motor driver (11 x 11 x 3.5 cm), the control panel (25 x 20 x 12 cm) plus their respective connections and some extra space. The devices on the top compartment would require the following dimensions: three cameras modules of approximately 25 x 23 x 9 mm, a single board computer (SBC) of 80 x 65 x 9 mm, two optic fiber sensors of 20 and 10 cm of height and extra space for actuators, wires and future sensors.

The most important part of an autonomous system are the sensors and the actuators. The sensors are separated in two categories according to their function. The first one is for data acquisition. This category consists of the vision system, that is the RGB, IR and Thermal cameras, the optic fiber sensors for the hyperspectral imaging and the humidity and temperature sensor. The other category is for positioning, this includes the limit switch and the RGB camera. Both sensors help to identify in which inspection point the cart is across the rails. The only actuator in the system is the motor that would move the cart forwards or backwards while on the rails.

The rail system in which the car will be navigating at Jornada's site consists of a straight rail-line of 110 meters, with markings every meter for sensing. They are of a standardized size, first used by John A. Gamon [4] and currently used in sites across Alaska, California and New Mexico among others. Although the terrain is very irregular, the rails are completely horizontal, having a little inclination, this helps to have a better control of the position and better measurements.

The new design needs to be a robust cart, capable of withstanding the conditions described in the previous paragraphs and summarized in Table 3.1. It also needs to be autonomous by

following schedules for measuring and with the capability of being accessed and rescheduled remotely. It will also have a charging port that should be able to engage with the docking station for charging when needed or when not in use. In addition, the compartments should be easy to access by the user to take back components, memory devices or sensors. And, it should be able to navigate along the rail line already installed at the JER's site.

Table 3.1. Tram Cart new design specifications

Compartment	
Top Compartment	Fit RGB, IR, thermal cameras, computer and optic fiber sensors
	IPX4 like protection
	Windows for cameras and optic fiber sensors
Bottom Compartment	Easy-to-access compartment
	Fit UniSpec-DC, 12v batteries, Motor driver, control panel
	IPX4 like protection
Structure	Withstand 20 mph winds
	Charging port

3.2 New Design

One of the major requirements for the design is that it should be easy to replicate, and replacements should be easy to obtain for remote locations. This means opting for commercial parts when possible instead of customizing them to fit a specific design because this could lead to delays in construction of new units or in hard-to-find spare parts. Because of this, most of the components of the cart are commercial branding.

For the cart structure, the aluminum extrusions from T-Slots are used. These use structural aluminum 6560 alloy and have the profile and dimensions shown in the Figure 3.1. other specifications are shown in Table 3.2. The Figure 3.2 shows the behavior of an aluminum bar with

a uniformly distributed load cantilevered. This is the closest exemplification of the real loads that will affect the structure.

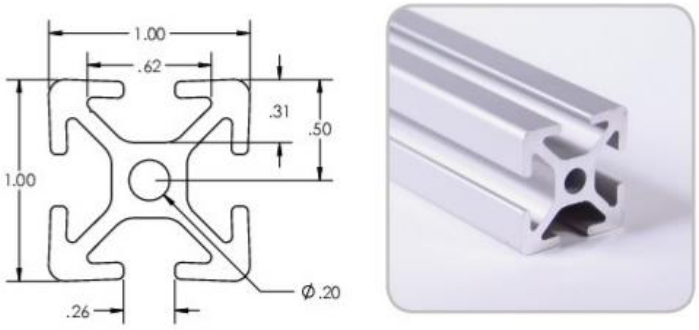

Figure 3.1 Aluminum profile used in Tram Cart.

Table 3.2. Aluminum extrusions technical specifications.

Property	Value
Alloy	6560, T6 Temper
Yield Strength	172 mpa = 25 ksi
Tensile Strength	206 mpa = 30 ksi
Elasticity (E)	10,000 ksi
Hardness	12 + Webster Model “B”

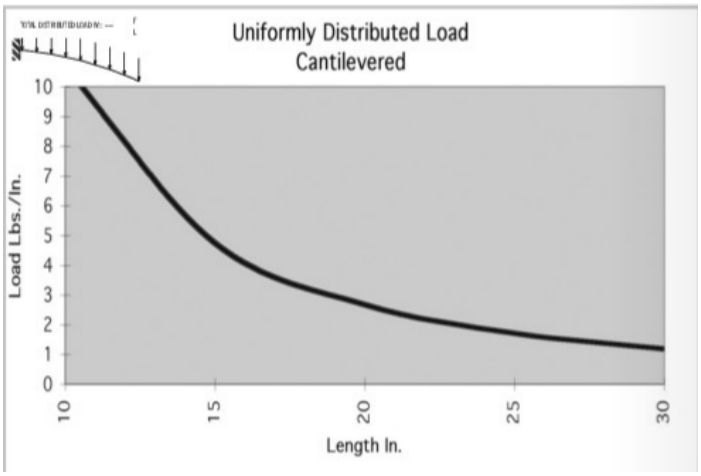

Figure 3.2 Uniformly Distributed Load Cantilevered

Figure 3.3 shows the structure design made with aluminum extrusions. As mentioned before this work is direct continuation of the presentation done by M.S. Emmanuel Ochoa [11] and the previous design was used to perform software tests. Because of that, this structure was used as the base for this project. Figure 3.4 shows some sketches of possible designs.

Figure 3.3 Cart structure using T-Slots aluminum extrusions

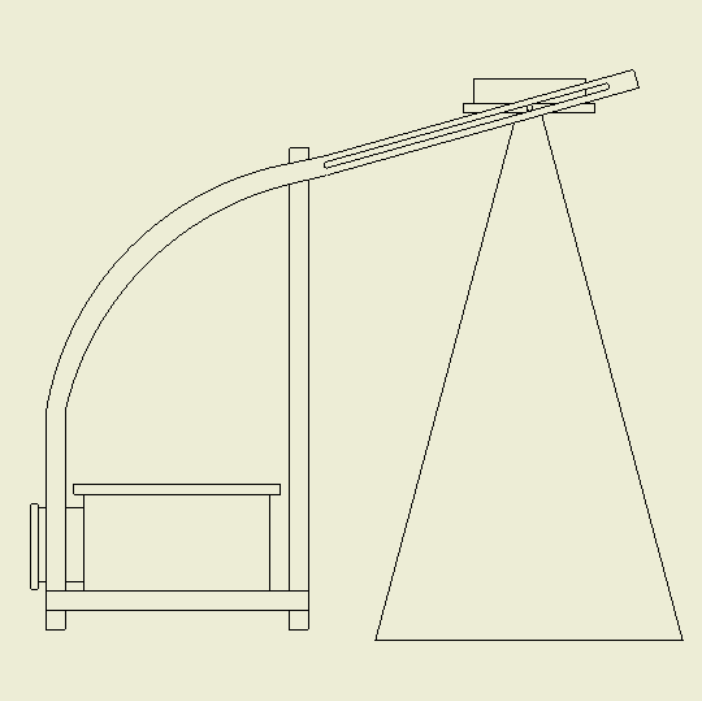

Figure 3.4 Alternative designs

The first thing done was to digitalize the design. Every bar was measured to recreate an accurate replica of it for documentation and simulations. Figure 3.5 shows the drawing for the tram unit. Once all the dimensions were acquired the search for the rest of the components and the design of the compartments started. On the next sections the rest of the tram unit compartments are going to be described starting with the top compartment, then the bottom compartment, structure and finally the docking station.

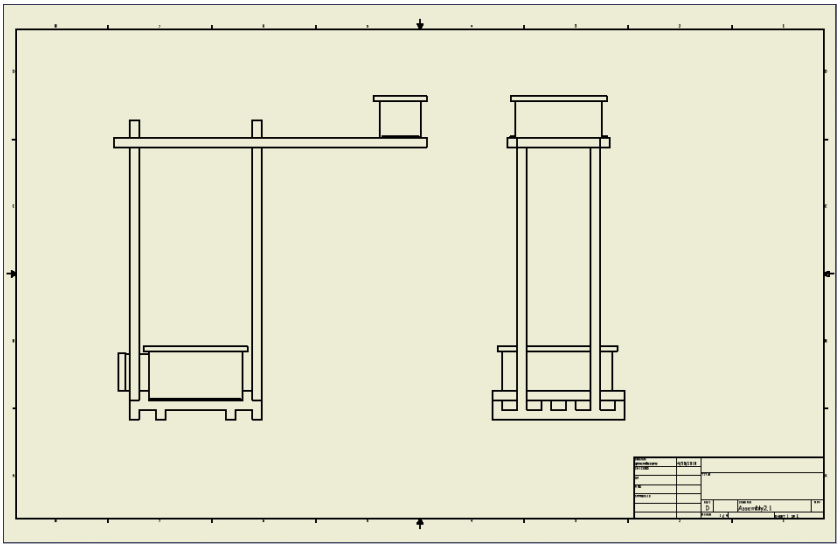

Figure 3.5 Tram unit drawings.

3.2.1 Compartments

As mentioned the Cart will have two compartments, one on the top of the structure that will hold most of the measurement instruments and one on the floor level with the batteries, the multi-spectrometer among other instruments. Both compartments must have an ingress protection similar or greater than the IPX4, endure temperatures from 0 C to 60 C and have easy access to the inside for component replacement or maintenance.

The top compartment needs to enclose the following components (Figure 3.6): Two fiber optic sensors, for hyper-spectral imaging, an RGB, near-IR and Thermal camera, a raspberry pi as a controller computer, a communication hat that works as an interface between the sensors and the computer, some actuators and all the connections.

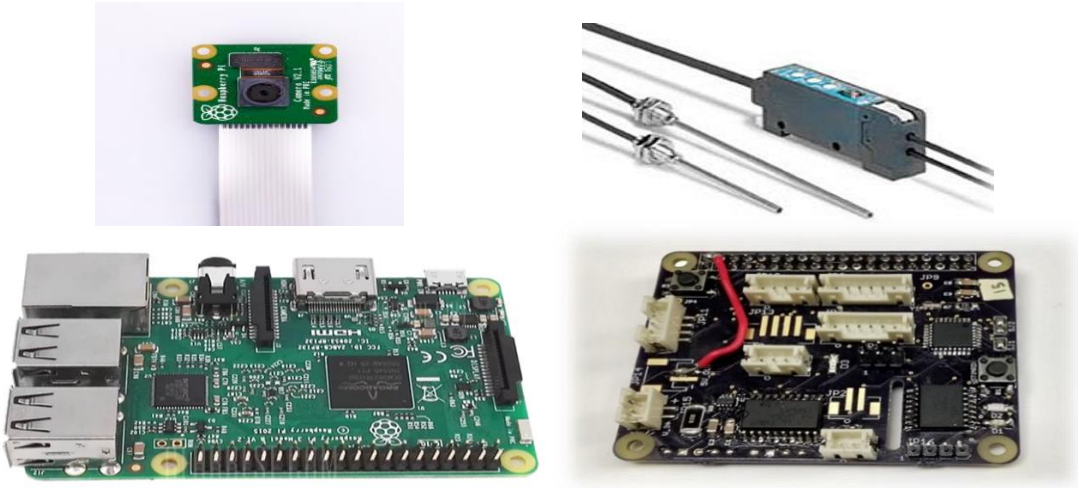

Figure 3.6 Electronic components for data recollection

For functionality, the compartment must keep the component safe from the environmental conditions of the desert while not in operation. In addition, it must have opening mechanisms for both optic fiber sensors. As it takes measurements in a great part of the Electromagnetic spectrum, no window can be used for them because it may block or distort some wavelengths adding noise and uncertainty to the data. It also needs two clear windows for the RGB and near-IR cameras and a germanium window for the thermal camera, this allows the recording of specific wavelengths. When positioning the sensors these must be as close as possible to each other, this to allow capturing the same area with all the sensors. Finally, it must have enough space for all the previous components plus some extra space for future projects.

To meet the needs the J1407HPL case from Stahlin enclosure was selected. It is a case made of molded fiberglass reinforced polyester, especially designed for exteriors following the UL 746C standard, with stainless steel hinges and latches, self-extinguishing with a UL94-5V flammability rating and an ingress protection level similar to IP66 according to IEC 60529. The dimensions of the case are 14 x 7 x 6 inches, this allows it to fit on the arm extended on the top of the cart (Figure 3.7).

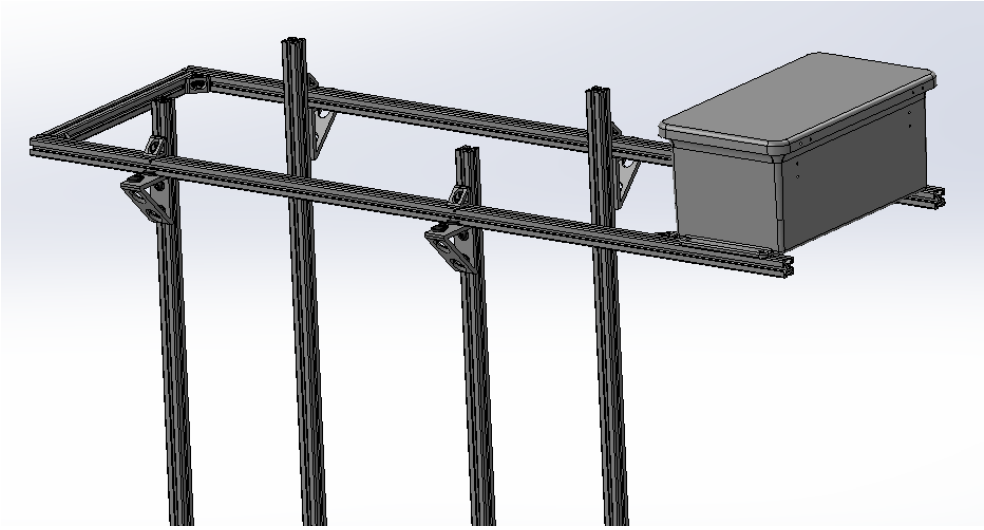

Figure 3.7 Top compartment

For placing all the components inside the case, a couple of aluminum perforated bars were placed, this to create a holed-floor like surface to place around the cameras, sensors and computer according to the needs (Figure 3.13 a). As mentioned before, an opening mechanism will need to be designed for the optic fiber sensors. The first attempt basically works as a door, it would have a spring that when extended the door will be open by ninety degrees, and then a motor should apply force to close and a solenoid would latch the door keeping it closed until the next scheduled task (Figure 3.8). This design had some problems first: it would need some custom pieces. A spring of the specific size, either a couple between the motor and a size of the spring, or a sort of threaded rail to close the door using only the motor rotation. Also, although the cart measures close to noon, in case the user decides to launch the cart at another time, the door itself could create a shade that would cause an erroneous reading. On the other hand, if it opens inwards it would require more space. Thus, this option was discarded.

Figure 3.8 Door-like mechanism for Optic Fiber Sensors.

The second option was using a single mechanism for both sensors instead of one for each. This will be achieved by attaching both sensors to the wall of the case, aligned and each one looking in their corresponding direction. Then a part of the case side, the one that has the sensors will come out a few centimeters moving the sensor to the outside allowing them to take measurements and when finished the sensors will return to the inside (Figure 3.9). This would require a slider with a pinion gear and a rack to control the movement of the "side lid" with the sensors, some sort of support extendable structure to keep the sensors from falling and to help guide the displacement of the lid plus a sensor for knowing when it is fully open and fully closed. This design was also discarded, mostly because it will over complicate the inside distribution and would leave a big hole on the side while operating that could allow animals into the case.

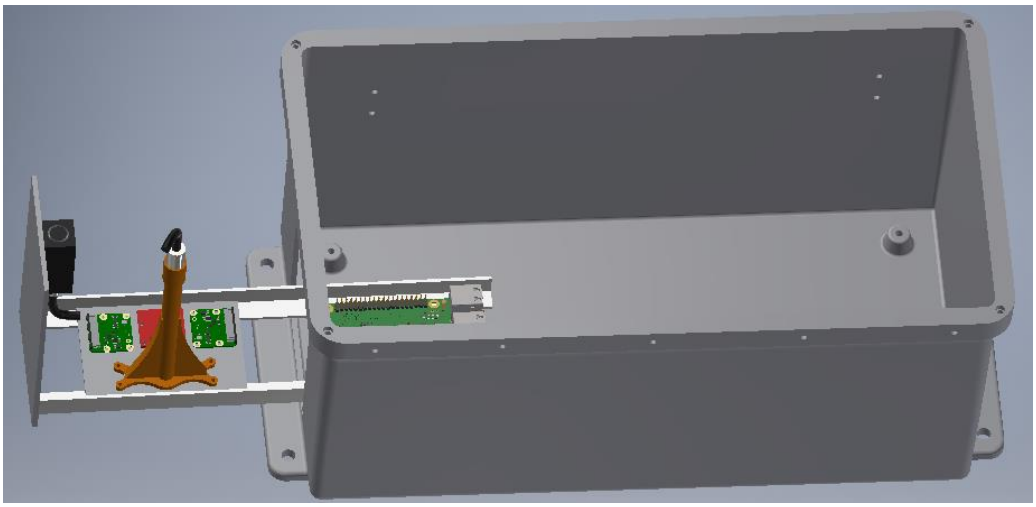

Figure 3.9 Side door mechanism for Optic Fiber Sensors.

After that, water bottles were taken as inspiration by trying to replicate their opening mechanism (Figure 3.10). This design would use a total of 4 links and the cap, two on the outside of the case and two on the inside, this was very complex and to get those links done in that dimensions would be hard, plus the links will cover part of the hole, interfering with the measurement. So, for the next iteration instead of replicating the structure it was opted to emulate its movement. For this one a cap with a curved rack was designed, it will have a servomotor attached that would move the cap upwards. The only problem was that the rack would be thicker than the links and would block the opening (Figure 3.10).

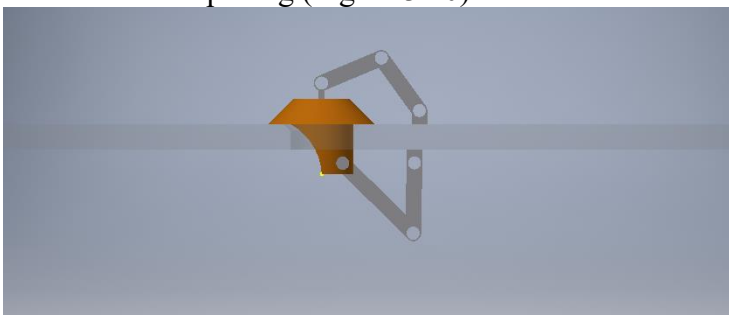

Figure 3.10 Links, bottle and racked cap

Using the cap idea and trying to replicate the simple sliding mechanism used for the sensor pointing down the design shown in Figure 3.11 was achieved. The mechanism is simple, is a custom cap and uses a solenoid. The cap is a conic cap with a cylindrical base of a smaller diameter

and a bar attached to its bottom, this allows the solenoid to be attached to it at a certain distance. But the hole on the lid is different this time, it is a regular hole, big enough for measuring but it has a slot on the side of a smaller diameter, this allows the base of the cap to travel across the slot uncovering the measurement hole completely. And when closed, the cap covers completely protecting the inside of rain.

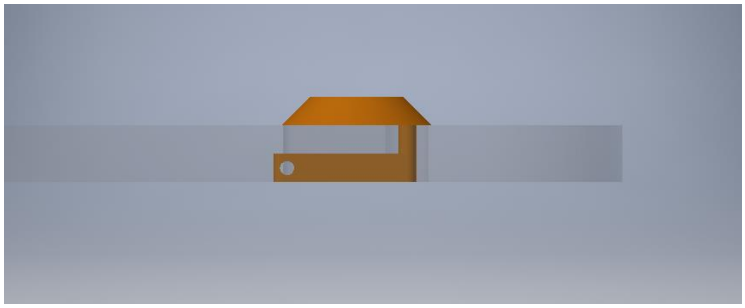

Figure 3.11 Opening mechanism for optic fiber sensor

Once the opening mechanism was chosen, it is time to place everything in the cases. To hold in place the optic fiber sensors, custom supports were designed (Figure 3.12) to be later 3D printed. One of the benefits of 3D printing is the ease of prototyping and customizing designs, this allowed to create supports that will fit our needs perfectly and if needed make modifications for future customization very simple. The rest of the components were placed as shown in figure 3.13. The cameras were attached to the aluminum plates, the computer is held by spaces and was positioned above the plates, the optic fiber pointing toward the ground is on the plates while the one pointing toward the sky is held by the box itself.

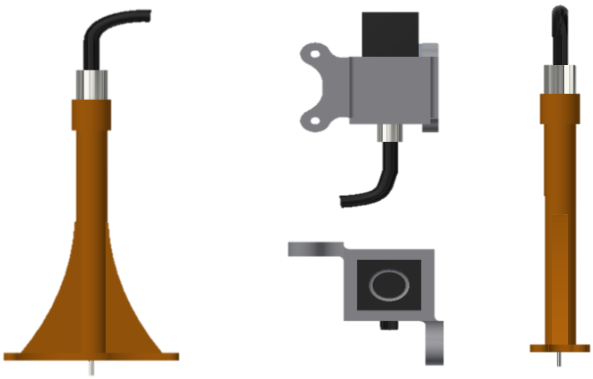

Figure 3.12 Supports for Optic Fiber Sensors.

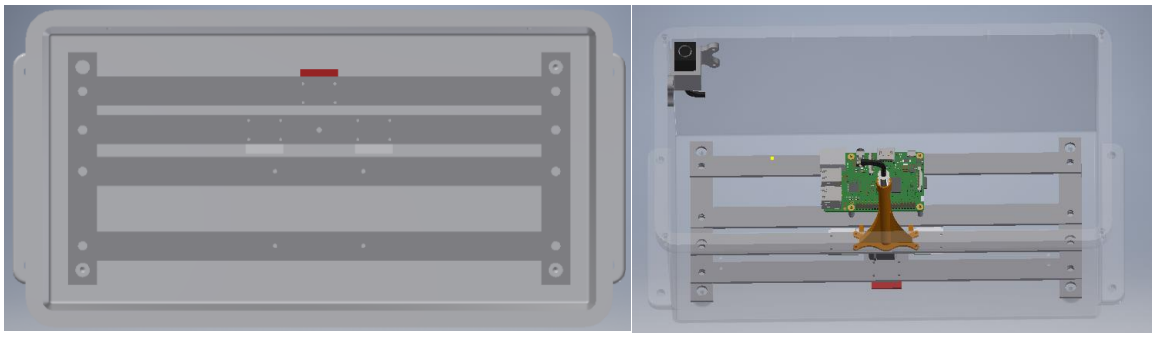

Figure 3.13 a) base of top compartment. b) Components inside top compartment.

For the bottom compartment, the J1816HL case from Stahlin enclosure is used. This one has the same characteristics as the one described above but the size, this one is 18 x 16 x 8 inches. For the components, it has an aluminum-perforated frame that allows screwing separators and brackets according to the number of sections and sizes desired (Figure 3.14). This case will contain the batteries, and the Unispec-DC computer. Also, the side will have attached the control panel. For this one the Pelican case 1150 was used. This case has a polypropylene body with an IP67 ingress protection and withstand temperatures from -40 C to 99 C.

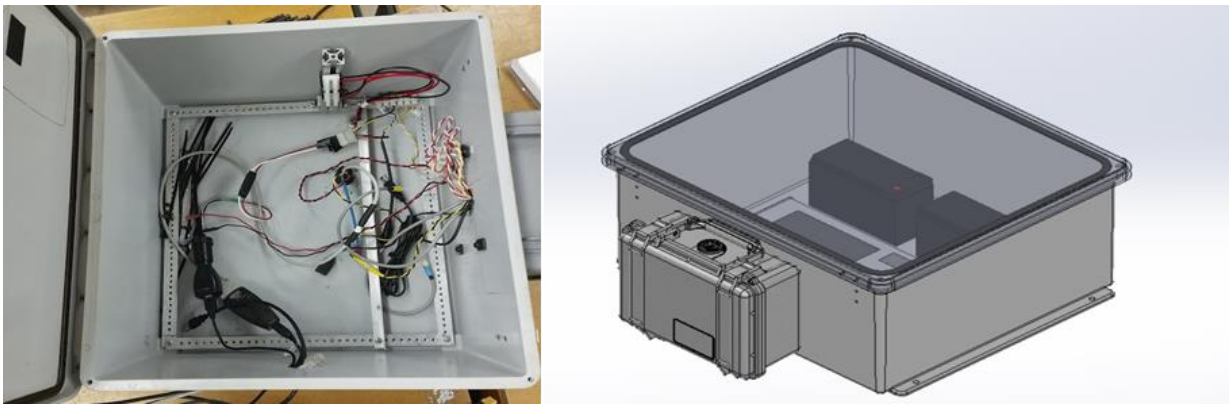

Figure 3.14 Bottom compartment

As mentioned previously, the structure is built of TSLOTs aluminum extrusions (Figure 3.15), and it needs to have a functional charging port, an Anti-detach mechanism and a way to protect the cables that go from the bottom compartment to the top one. It also needs to withstand

loads equivalent to winds of 44.739 miles per hour and move with ease through the rails. To see if the structure will meet these requirements the loads equivalent to a 44.739 miles-per-hour wind over the structure will be calculated and used in a structural analysis to get the estimated stresses on the tram unit as well as a Finite Element Analysis to corroborate the structural analysis.

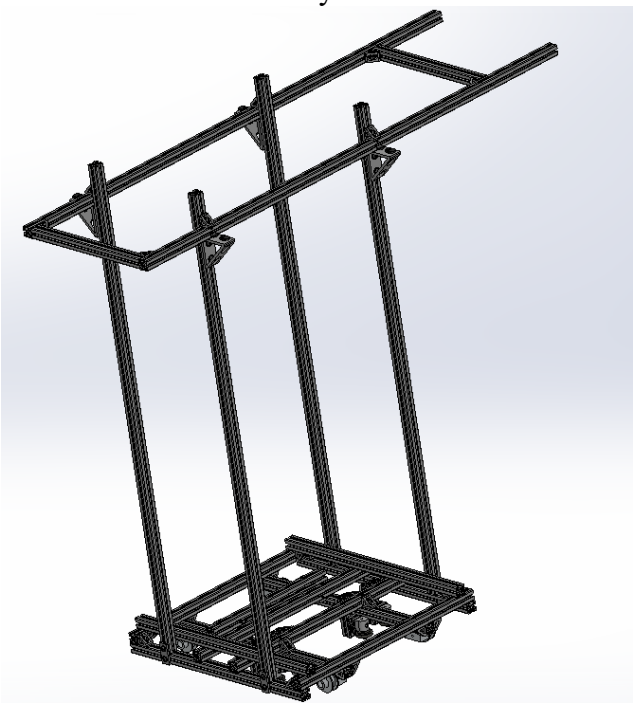

Figure 3.15. Tram unit structure

To avoid detachment from the rails, four roller wheels were used (Figure 3.16). These are positioned horizontally; this allows the cart to move freely along the rails in the horizontal direction but not on the vertical axis. This model has a brass bushing and supports loads of up to 50 lb. To help protect the cables that communicate between both compartments the Ultratite Type NM conduit was used. Which is a liquid tight flexible nonmetallic conduit with oil, sunlight and crush resistance and temperature rated -30°C to 80°C.

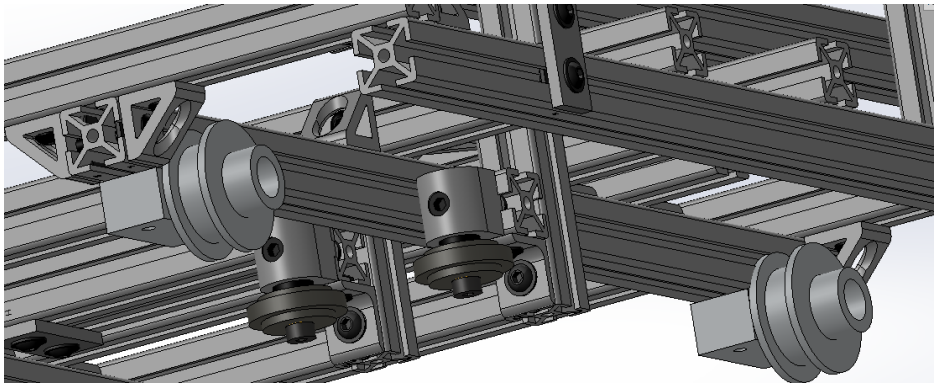

Figure 3.16 close up to anti-detach device.

When designing the charging port, first it was decided to use the one already installed on the cart while testing (Figure 3.17). These consist of a PVC tube with right angles on the top attached to the chassis of the cart. Right after the angle another section of PVC tubing extends and houses a car lighter connector. For this to work, the docking station must have a pair of car lighter sockets, each pair (connector-receptacle) carries one pole, meaning one would be connected to the positive part of the battery while the other to the negative connector. Like mentioned before, the connectors worked on testing, but they will not survive a long exposure outdoors. Therefore, another alternative must be selected.

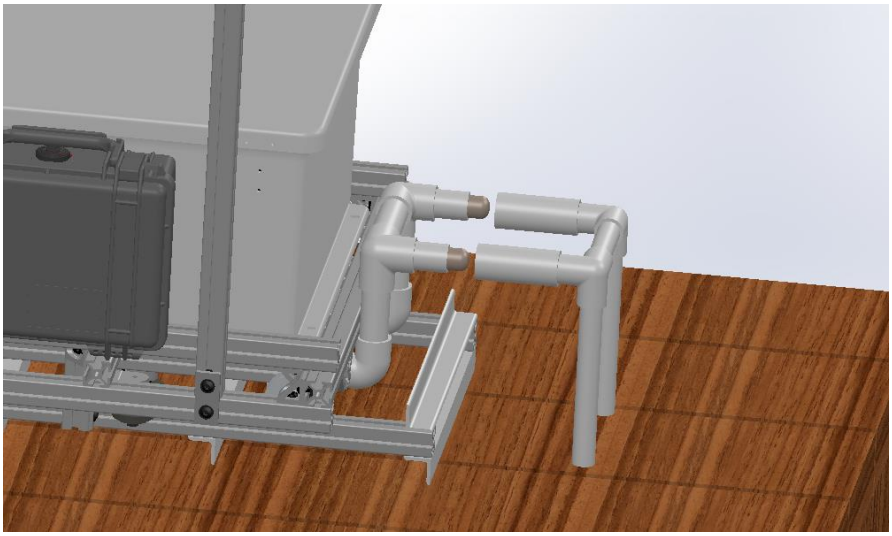

Figure 3.17 Charging ports first version.

The charging port was designed with the robotic vacuum charger in mind. Where two conductive plates are located on the charger at almost ground level and on the vacuum two retractable pins are located on its bottom with the same distance. When the vacuum goes into the base it attaches itself to it, making the pins go inside for a bit, but because of the spring that pushes them out they are in constant contact with the loaded plates allowing the robot to charge its batteries. Because the pin-spring-plate mechanism is going to be a little hard to customize for our unit, a wheel-plate pair replaced them (Figure 3.18). Because of the wheel itself will have bearing and grease, this option was not selected.

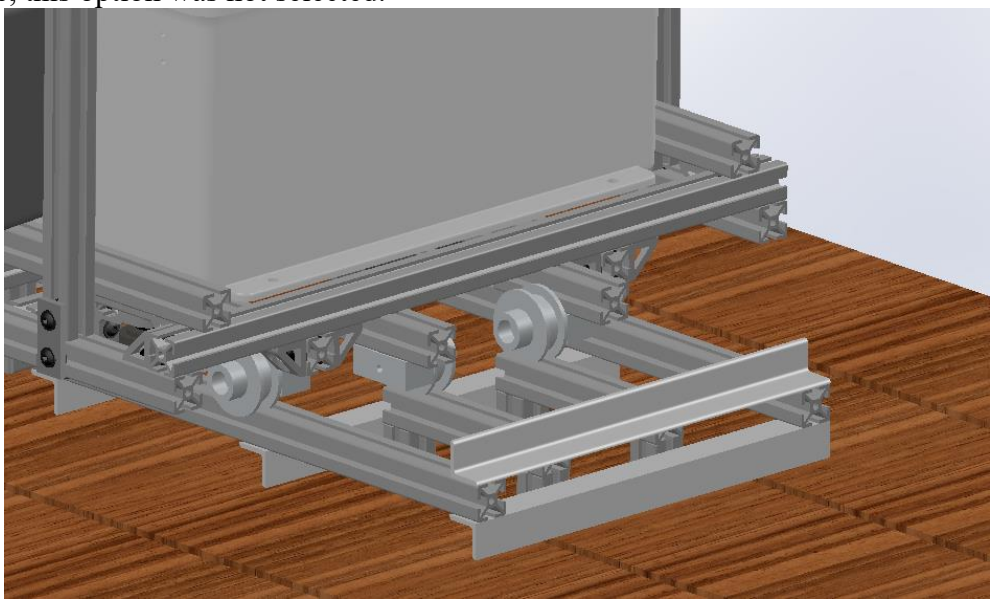

Figure 3.18 Wheel-Plate charging port

After that design, a more classic approach was taken, by looking and taking as base the blade switches. They have an old but yet functional and efficient design. A similar design was achieved by attaching two completely isolated plates to the structure, then connecting this to the battery controller, and on the docking station a “V” shape receptacle was placed (Figure 3.19). One of the benefits of this design is that even if it is made of brass, it will require very low maintenance and having no moving mechanical parts the chances of failure are reduced. One of the problems that most designs have is that when electricity passes through a connection made

with two different metals it creates corrosion. This corrosion can be avoided or reduced following certain recommendations that would be discussed later.

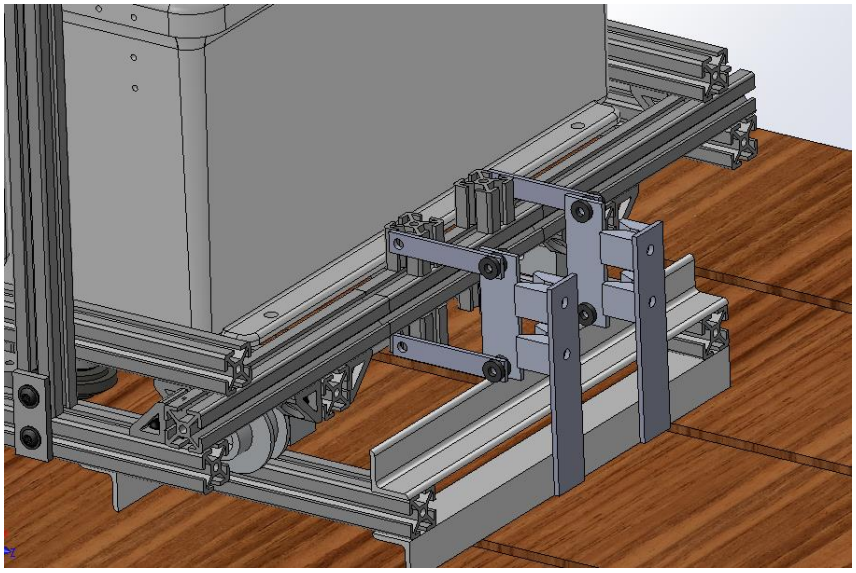

Figure 3.19 Blade Charger.

Chapter 4: Structural Analysis

Structural analysis is a tool to determine the effect of external forces on a physical structure and its elements [12]. To perform structural analysis two things must be defined. First is the structural form or design of the structure to analysis, its supports, the type of elements and connections it will have, and the material and properties of said elements. Second is the loads the structure will have to support. The type of loads, their magnitude, their direction and location across the structure. The design of the structure was defined in the previous section (Figure 4.1) as well as the materials used and some of the connections, but it will be explained in more detail in the following sections. As for the loads, the only ones specified are the loads equivalent to wind of 44.739 miles per hour (20m/s), which is the only external load affecting the system, but more internal forces need to be addressed for solving this analysis. All the forces involved in the analysis will be defined and describe later. Once the loads and the structure itself have been defined, some considerations and limitations for the supports and connections will be addressed to solve the analytical method.

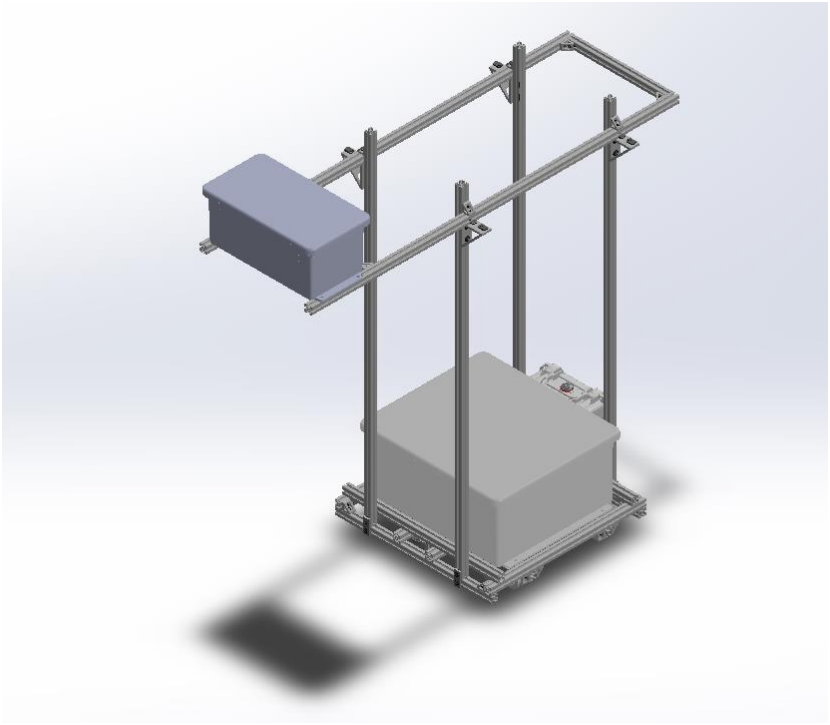

Figure 4.1. Tram Cart Structure Design

4.1 Structure definition

The first step in structural analysis is to define the structure that will be subject to loads. In the last chapter the structure design was described as well as the material used. Now it is time to identify the types of elements composing it. The three main types of structure elements are: Tie Rods, Beams and Columns. The Tie Rods or bracing struts, are structural members subjected to tensile forces, and due to these loads these members tend to be rods, bars, angles or channels [12], (Figure 4.2). Tensile forces are forces applied at the ends of the member, directed along the members axis and that elongate the member.

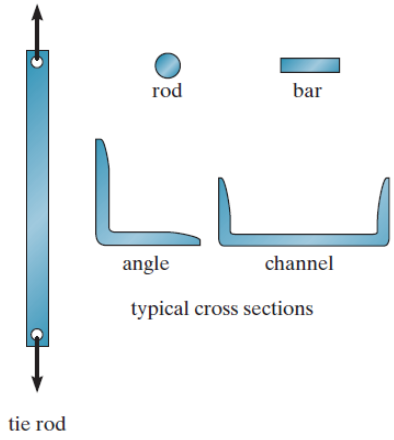

Figure 4.2 Tie rods examples

Beams tend to be straight horizontal members subjected to vertical loads, as the tie rod their cross section can have various shapes (I-Beam, T-beam, Channel, rectangular). Beams are mostly designed to resist bending moment and are often classified based on their supports (Figure 4.3).

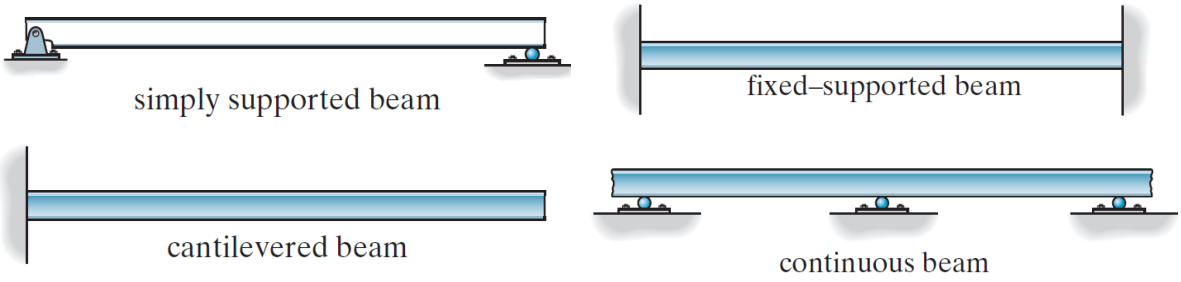

Figure 4.3 Different supports for beam elements.

Lastly, the columns, these are members are like the tie rods, vertical elements subjected to axial loads, but these loads are compressive loads. Some columns are supporting a combination of an axial load and a bending moment. These columns are known as beam columns (Figure 4.4).

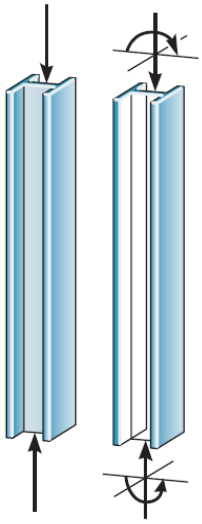

Figure. 4.4 Columns

Now that we know basic types of structures element it is time to define the element from which our cart is made. Although most elements are 6560 aluminum extrusions, they experience different loads in different ways. Starting from the top, the two horizontal elements will be considered as beam elements, because they are carrying the enclosure on one side and have two supports (Figure 4.5).

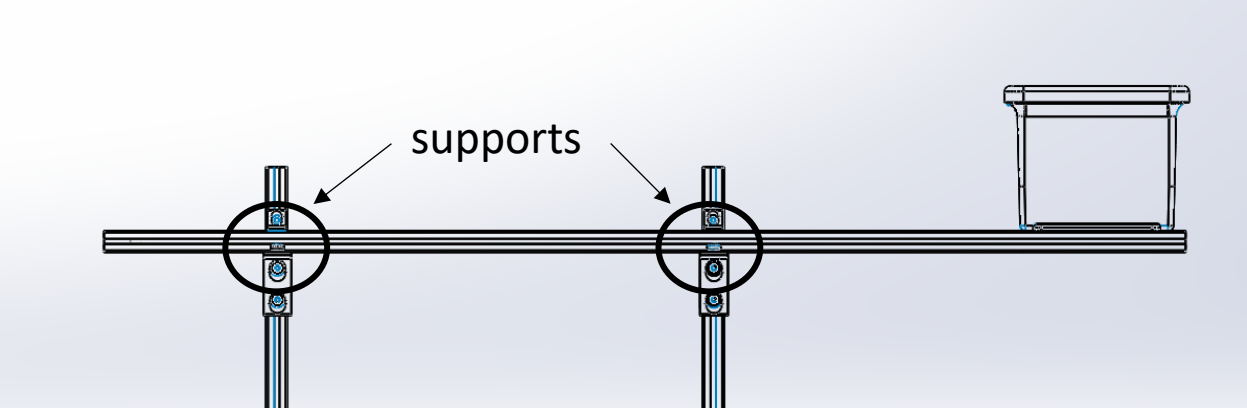

Figure 4.5 beam elements at top of tram cart.

The four long vertical elements act as beam columns, because of the loads they are subjected to as well as the four elements holding the anti-detach mechanism and the ones holding the wheels at the bottom of the system. The rest of the horizontal elements at the lower section of the cart are considered as beam elements (Figure 4.6). The only horizontal elements acting as a tie rod are the short ones at the top, their only function is to keep the two large ones together by increasing the stiffness of the structure.

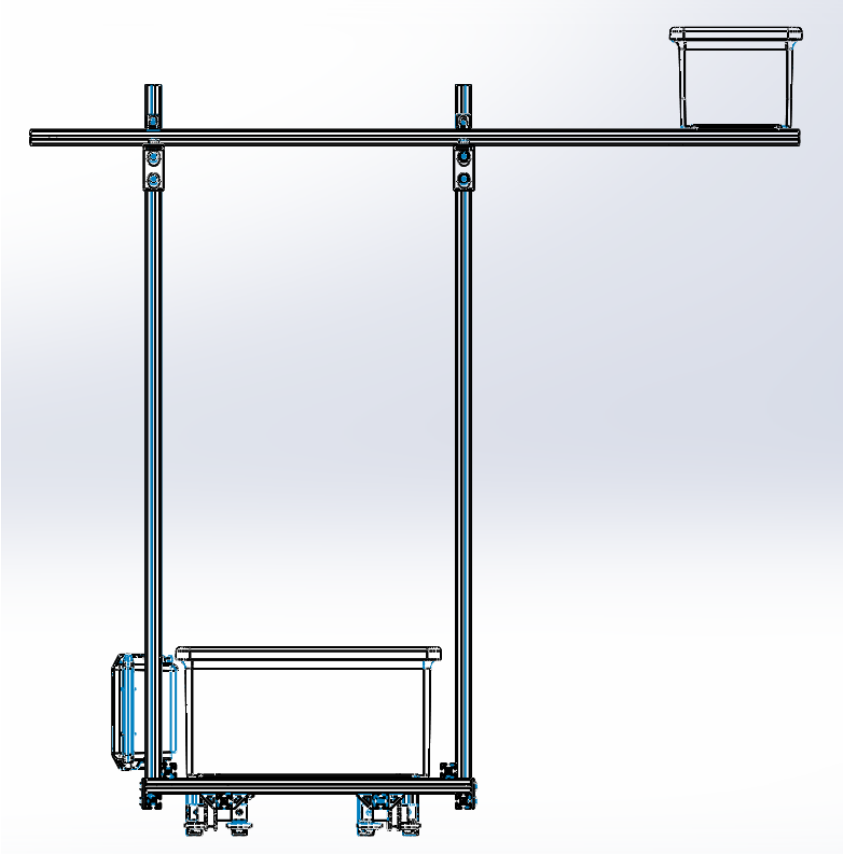

Figure 4.6 Structure elements.

4.2 Loads definition

The structure design, its elements and its dimensions have been defined. The only thing missing for a structural analysis is to declare the loads the system will need to withstand. As elements there are also several types of loads, dead loads, live loads, building loads, impact loads, wind loads, highway and railroad bridge loads among others. For this analysis, our structure will only be subjected to dead loads and wind loads. Dead loads are nothing more that the weight of all

the structural members and any other object that is going to be attached permanently to the structure. Table 4.1 shows the combination of some members and theirs weight.

Table 4.1 Tram carts components weight.

Element	Weight
Top Compartment	6 lb
Structure (cont. all aluminum extrusions members)	24.437 lb
Bottom Compartment	20 lb

Wind loads happen when a structure blocks the flow of wind, transferring the wind's kinetic energy to the structure as potential energy of pressure [12]. To calculate a wind load, one must know the density and velocity of the air, the angle of incidence, the contact surface and the structure shape. These loads can be treated as static or dynamic. For this analysis the loads are going to be static. The pressure transferred can be calculated with the equation 4.1. Where q is the dynamic pressure, ρ is the airs density and V is its velocity. The ASCE 7-10 Standard add some modifiers to the equation to account for its height (K_Z), the risk of human life and the terrain where is located (K_{Zt}) and the direction of the wind (K_d) (eq. 4.2). For this equation, the velocity (V) depends on the category of structure. For example, 105m/h for agricultural or storage building and 120 m/h for hospitals. As our structure present will not endanger human life, is located in a plain terrain and at relatively low height, equation 4.1 will be use for the analysis.

$$q = \frac{1}{2}\rho V^2 \quad eq.(4.1)$$

$$q_z = 0.00256 K_Z K_{Zt} K_d V^2 \quad (lb/ft^2) \; eq.(4.2)$$

4.3 Calculations

Now that the structure and the loads to which it will subjected are defined, it is possible to start the analysis. The first step is to draw a free body diagram with all the forces and supports involved. Figure 4.7 shows the free body diagram of our system. The arrows represent the forces affecting the structure. The horizontal forces represent the wind loads while the vertical arrows are the dead loads on the system.

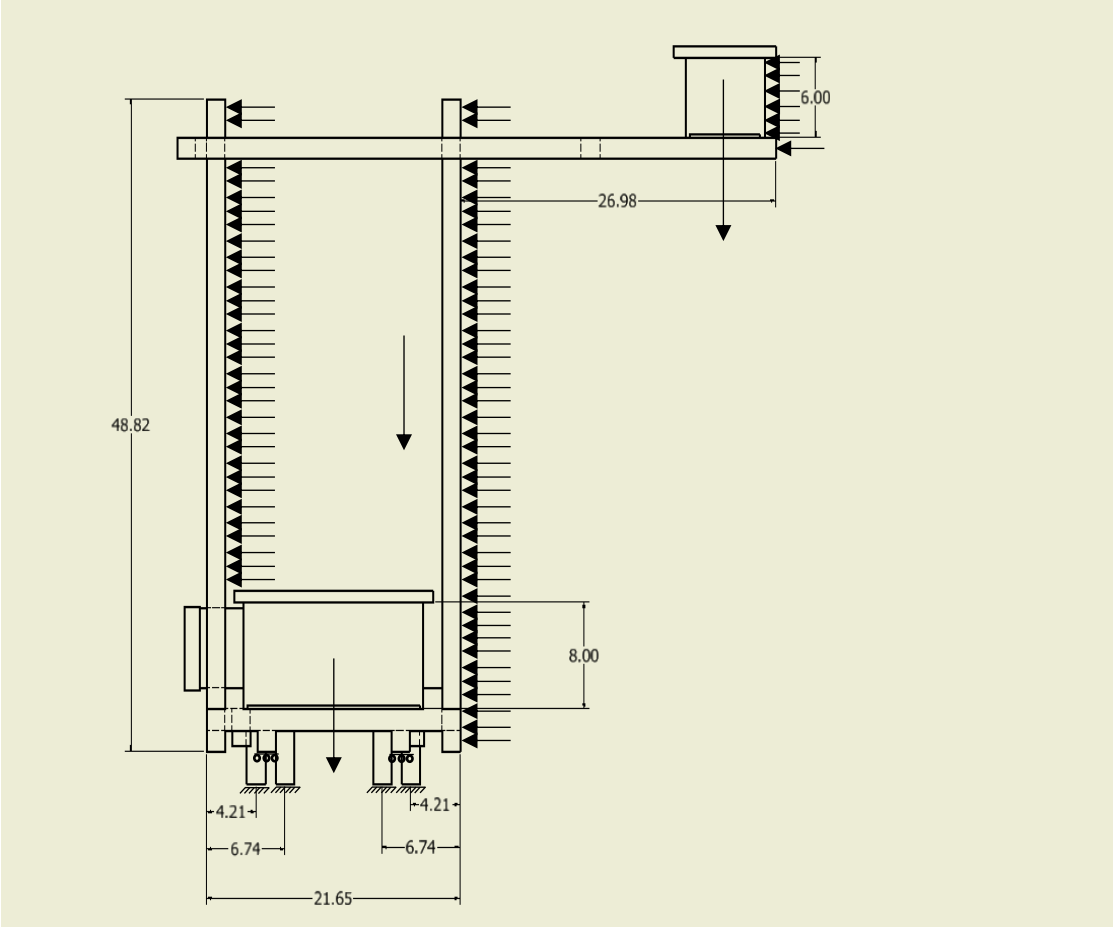

Figure 4.7 Free Body Diagram of the structure.

To calculate the pressure produced by the wind at 44.739 miles per hour (20 m/s) the equation 4.1 is used. The air density (ρ) is taken as 0.0780 lb/ft^3 (1.225 kg/m^3) which is the density at room temperature and sea level. The velocity is 44.739 miles (20m/s) and it gives a dynamic pressure of 245 Pa (N/m^2) or 0.0355 psi.

$$q = \frac{1}{2} * 1.225 * 20^2 = 245\ Pa\ or\ 0.0355\ psi$$

Once we have the pressure the loads in each element can be calculated and position on the free body diagram. To do that the areas of the contact surface of each element need to be calculated and once that is done just multiply the pressure by the area to get the point force equivalent to the air pressure. The table 4.2 shows the elements with their respective areas and the forces acting on them.

Table 4.2. Forces acting in each structural element.

Element	Area ($inch^2$)	Force (lbf)
Top Compartment	85.2501	2.9674
Lower Compartment	141.0502	4.9098
Vertical bars (4)	74.40014	2.5897
Horizontal Lower Bar (2)	34.2550	1.1923
Horizontal Top Bar	26.5050	0.9226

After calculating all the forces, it is time to position them in the correct place. For the wind loads, they need to be place on the center of the two-dimension surface that is stopping the air flow. The weights of the elements are positioned on the center of mass of each element. For simplicity, the structure was divided in three big elements, the frame, the top and bottom compartment. This allows to place only three forces going down that correspond to the weights of in element. Figure 4.8 shows the free body diagram with all the final loads and its magnitudes.

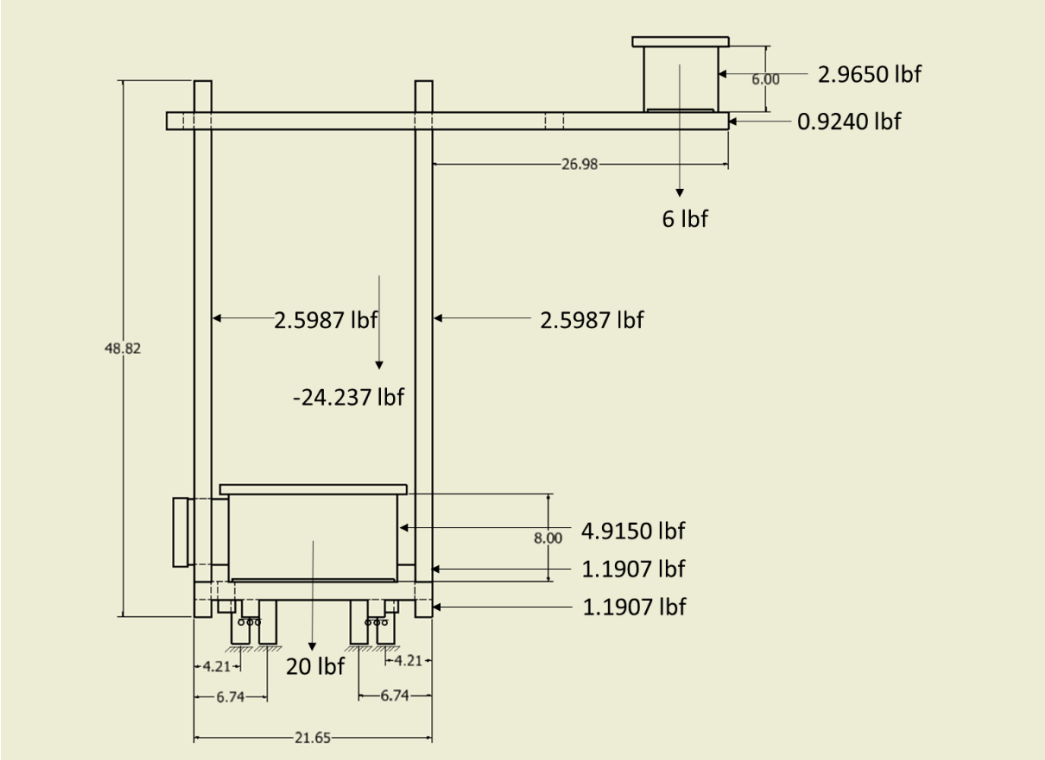

Figure 4.8. Free Body Diagram simplified with forces and supports.

Using the free body diagram above the structural analysis was performed focusing first on the top frame (Figure 4.9) to calculate the reaction forces on its supports. The first step was to set an origin point and get the coordinates for all the points of interest and its reaction forces. In this case, there are 5 points of interest (Pa-Pd, Pw).

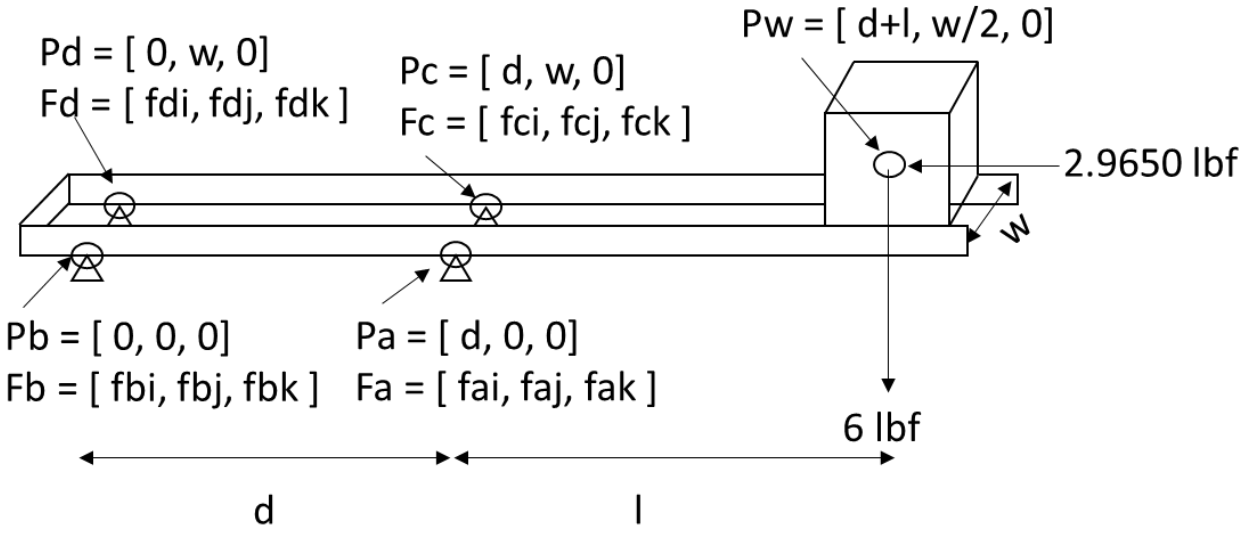

Figure 4.9 Top frame Free Body Diagram

Forces Coordinates	Forces
Pa = [d 0 0]	Fa = [fai faj fak]
Pb = [0 0 0]	Fb = [fbi fbj fbk]
Pc = [d w 0]	Fc = [fci fcj fck]
Pd = [0 w 0]	Fd = [fdi fdj fdk]
Pw = [(d+l) w/2 0]	Fw = [fwi fwj fwk]

Using the summation of moments and forces it is possible to get 6 equations. This leaves a system of equations of 6 equations and 12 unknowns. These equations are the summation of all forces in each direction (x, y, z) and the summations of moments around each direction. All equations in terms of the 12 unknown forces. To achieve this using MATLAB the points and forces

were defined as vectors and the moments are compute as the cross product of each point and its force vector.

```
% Moments
Ma = cross(Pa,Fa);
Mb = cross(Pb,Fb);
Mc = cross(Pc,Fc);
Md = cross(Pd,Fd);
Mw = cross(Pw,Fw);

% Forces and Moments Eq.
Feqn = Fa + Fb + Fc + Fd + Fw - 0;
Meqn = Ma + Mb + Mc + Md + Mw - 0;

% Eqn. Matrix
eqns = [Feqn(1) == 0    Feqn(2) == 0
        Feqn(3) == 0    Meqn(1) == 0
        Meqn(2) == 0    Meqn(3) == 0];
```

At this time the problem has 12 unknowns and 6 equations, to be able to solve it there are needed another 6 equations. To achieve this, Hooke's law is used (eq. 4.3) that says that the stress (α) is equals to the Young's modulus (E) times the normal strain (ϵ) (eq. 4.4). Adapting this equation to the problem we change the stress (α) its equivalent in terms of loads (F) (eq. 4.5).

$$\alpha = E * \epsilon \quad eq.(4.3)$$

$$\epsilon = \frac{l - l_0}{l_0} \quad eq.(4.4)$$

$$\alpha = \frac{F}{A} \quad eq.(4.5)$$

Substituting equation 4.5 and 4.4 into equation 4.3 we obtain equation 4.6. which will be used to solve this problem. The first part of the equation 4.6 is also known as the spring constant (k), substituting this and simplifying we are left with equation 4.7.

$$F = \frac{E * A}{l} * (l - l_0) \quad eq.(4.6)$$

$$F = K * \Delta L \quad eq.(4.7)$$

The datasheet of the material specifies that it has a Young's modulus of 10,000 ksi, close to 69 GPa and a cross-sectional area of 0.457 in^2 we can calculate the spring constant (K) for

each element (table 4.3). Using this extra set of equations, we end it up with 24 unknowns and 18 equations.

Table 4.3 Spring's equations

fak = kz * za	faj = ky * ya	fai = kx * xa
fbk = kz * zb	fbj = ky * yb	fbi = kx * xb
fck = kz * zc	fcj = ky * yc	fci = kx * xc
fdk = kz * zd	fdj = ky * yd	fdi = kx * xd

Because we are considering our structure as a rigid body, we can make use of the rigid body equation (eq. 4.8) which allow one to compute the position of one point with respect to another in terms of the rotations the body is subjected to. This equation states that the point A is equal to the point B plus the cross product of the rotation vector and the relative position vector.

$$\overrightarrow{X_b} = \overrightarrow{X_a} + \overrightarrow{\theta} x \overrightarrow{X_{a/b}} \qquad eq.(4.8)$$

Using these equations, we get 3 new unknowns, that are the rotations in each direction making a total of 27 unknowns. But we finish with 9 more equations (table 4.4). Having 27 equations and 27 unknowns we are able to finally solve the system.

Table 4.4 Rigid Body Equations

xa = xb	xc = xd – (dz * w)	xd = xb + (dz * w)
ya = yb + (dz * d)	yc = ya + (dz * d)	yd = yb
za = zb – (dy * d)	zc = zb – (dy * d)	zd = zb + (dx *w)

Writing all these equations into a MATLAB script and running it to solve it gives the reaction forces for the four points of interest. Having these forces, we can compare with the material properties to see if our structure will fail or will perform correctly on the field with this specifications and considerations. Table 4.5 Show the results from MATLAB.

Table 4.5 Results

Unkns	Force (lbf)
fai	0.74175
faj	0
fak	-7.4257
fbi	0.74175
fbj	0
fbk	4.42572
fci	0.74175
fcj	0
fck	-7.4257
fdi	0.74175
fdj	0
fdk	4.42572

To validate the code and equation system to solve the structural analysis a FEA simulation has been done using the simulation tool on SolidWorks. The next section will give a small introduction to the Finite Element Analysis and walkthrough the analysis.

Chapter 5: Finite Element Analysis

The Finite Element Analysis (FEA) consist in discretizing a continuous elastic structure into small but finite, well-defined, elastic sub-structures (elements) (Figure 5.1). Each element has the properties of the materials and a defined geometry that helps keep track of changes across the structure. The elements are defined by nodes, which are share with the element neighbors and are responsible of transferring loads, displacements and changes in properties as temperature, deformation among others. There are multiple applications for FEA for example stress and deflection, free or forced vibrations, heat transfer, acoustic, fluid dynamics and Multiphysics [13]. We will be using only stress and deflection approach for this analysis.

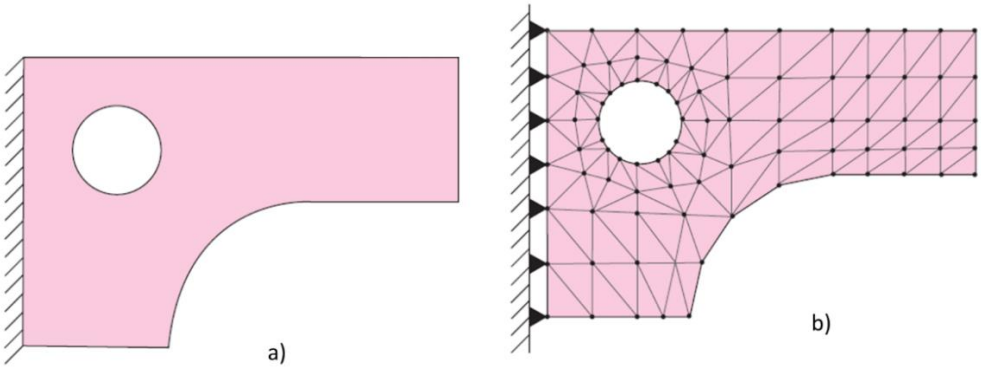

Figure 5.1 a) Model; b) finite-element model

5.1 Model description

The first analysis was performed on the SolidWorks assembly file (Figure 5.2) but because of the high detail the software generated a mesh with more than nine million nodes. As an educational institution, we have student license for this type of software and this license will analysis bodies with no more than 512 thousand nodes. Even selecting a very course mesh and changing the minimum and maximum element size it did not reduce the number of nodes below 512 thousand.

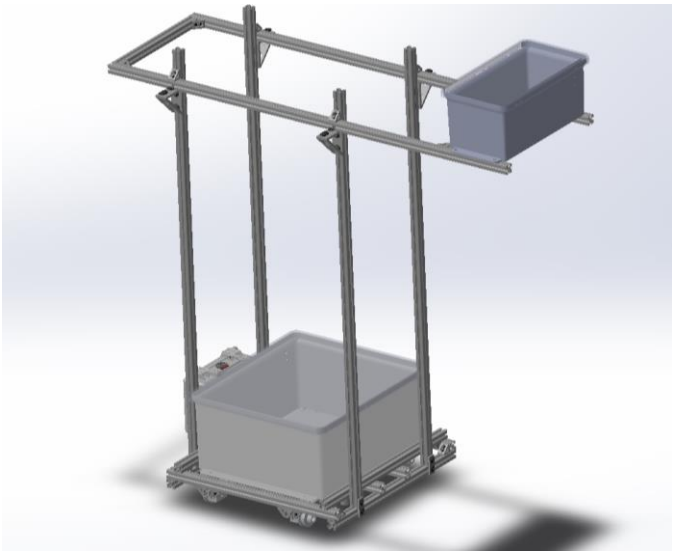

Figure 5.2 Tram Cart CAD assembly

The structure above was not meeting the software requirements, not even with using planar symmetry. Because of this, the CAD was modified to reduce all the small details it had. All the fillets, chamfers, hinges, screws, curvatures were removed, the compartments were replaced by square boxes of the same dimensions, and the aluminum extrudes were changed for rectangular bars (Figure 5.3). This allowed the software to generate close to 110 thousand nodes and a very fine mesh.

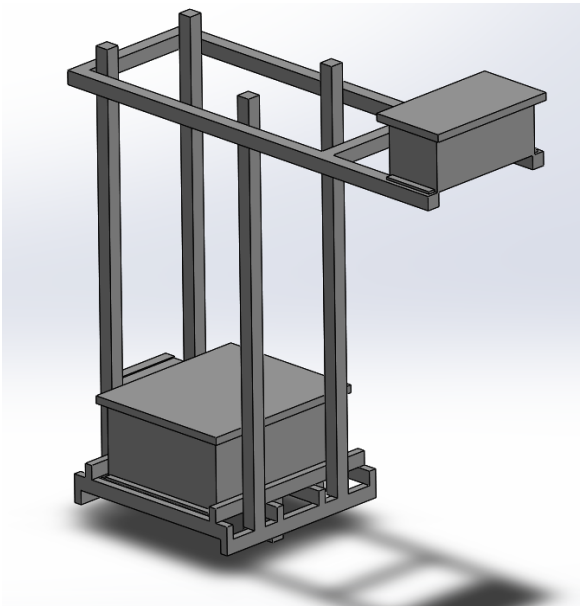

Figure 5.3 Tram Cart simplify CAD

5.2 Mesh

Mesh in FEA, can be defined as the network of nodes and elements that discretize a body or a section of a body [13]. The Simulation module of SolidWorks has very simple customization options for the mesh. The First one is “Mesh Density” that goes from coarse to fine, along with that option it lets you set the global size or the maximum size for the elements. The module has three types of mesh, Standard mesh, Curvature-based mesh, and blended curvature-based mesh. As default, the mesh generated is of the standard type, with a medium density and a global element size of 0.0842 ft (0.02568 m). This default mesh configuration gives a very coarse mesh, with 15928 nodes and 7782 elements. Figure 5.4 show the mesh generated with the default values.

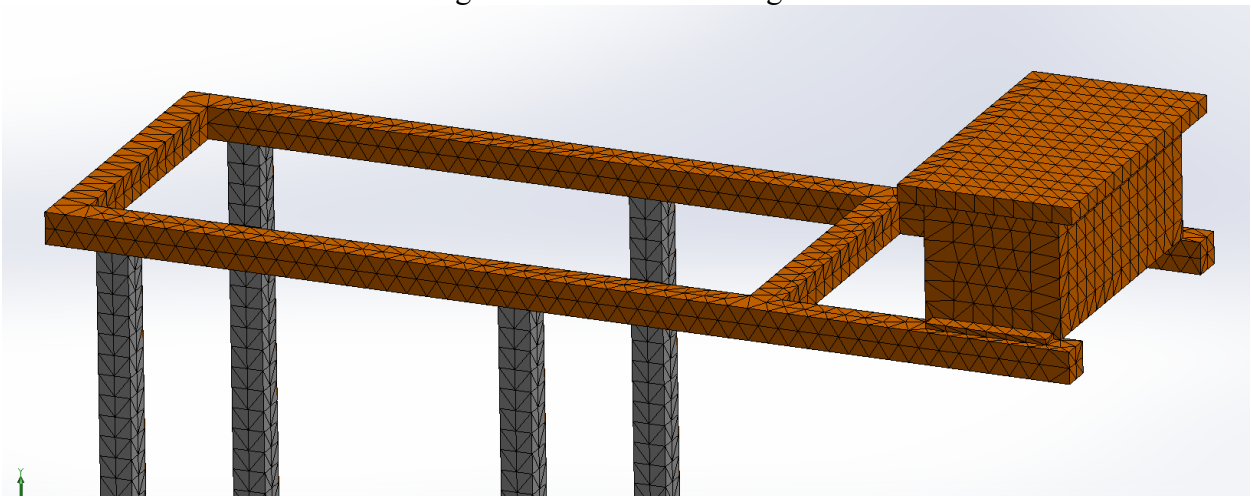

Figure 5.4 Default mesh generated by SolidWorks

Normally to increase the accuracy of your mesh it is recommended to increase the density of the mesh in areas of high stress or the mesh smoothly where the geometry changes. SolidWorks has an option called “Mesh Control” that will leave your mesh any entity independently from the rest of the body. The entities can be faces, vertices, edges, bodies. Figure 5.5 shows a comparison of the default mesh against the refined mesh using “Mesh Control” option.

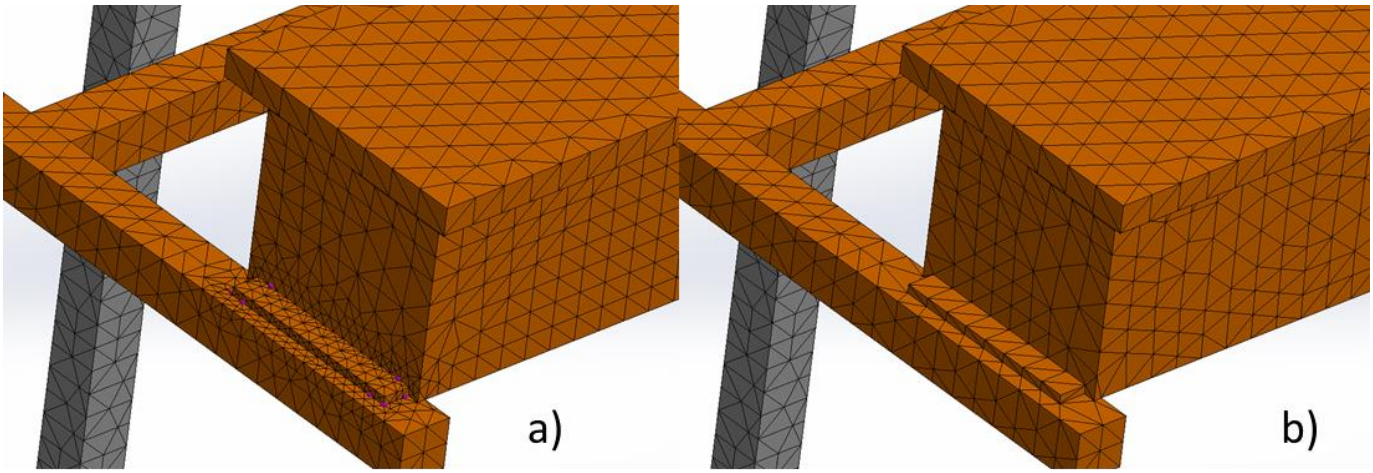

Figure 5.5 a) Default Mesh; b) Refined Mesh using “Mesh Control”.

After trying a couple of combinations, changing the type of mesh, the size of elements and using the Mesh Control option the selected mesh was a Curvature-based mesh with 112,166 nodes and a maximum element size of 0.0419 ft (0.0128 m) on the body and 0.0105 ft (0.00321 m) in the areas of high stress. Six areas of high stress were selected, the two connections between the top compartment and the top frame and the 4 connections between the top frame and the vertical bars. Figure 5.6 shows the final mesh with its properties.

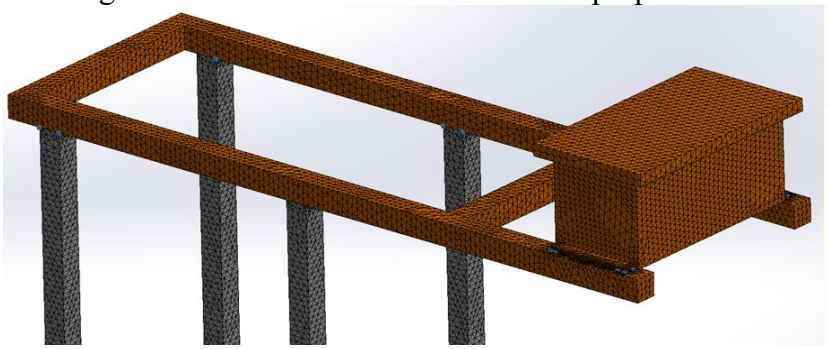

Study name	Static 1 (-Default-)
Mesh type	Mixed Mesh
Mesher Used	Curvature-based mesh
Jacobian points	4 points
Jacobian check for shell	On
Mesh Control	Defined
Max Element Size	0.0128417 m
Min Element Size	0.0128417 m
Mesh quality	High
Total nodes	112166
Total elements	63926
Remesh failed parts with incompatible mesh	Off
Time to complete mesh(hh:mm:ss)	00:00:04
Computer name	ADELLITA

Figure 5.6 Final Mesh for structural analysis.

5.3 Loads

Once the mesh is set the only things left is to specify the loads affecting the system. Because the main objective of this simulation is to validate the code presented in the previous section, only the loads used in that section will be placed. The load used was of 2.9650 lbf or 13.2 N. The

simulation module has a couple of options for loads, point load, torque, pressure, gravity, centrifugal and bearing load. As described in the previous section the load of 2.9650 lbf is the equivalent of the wind at a speed of 44.739 miles per hour, but it's also the equivalent of the pressure caused by the wind that is a pressure of 0.0355342 psi. So instead of using a point load we will be using the option of pressure and placed on the face of the top compartment (Figure 5.7).

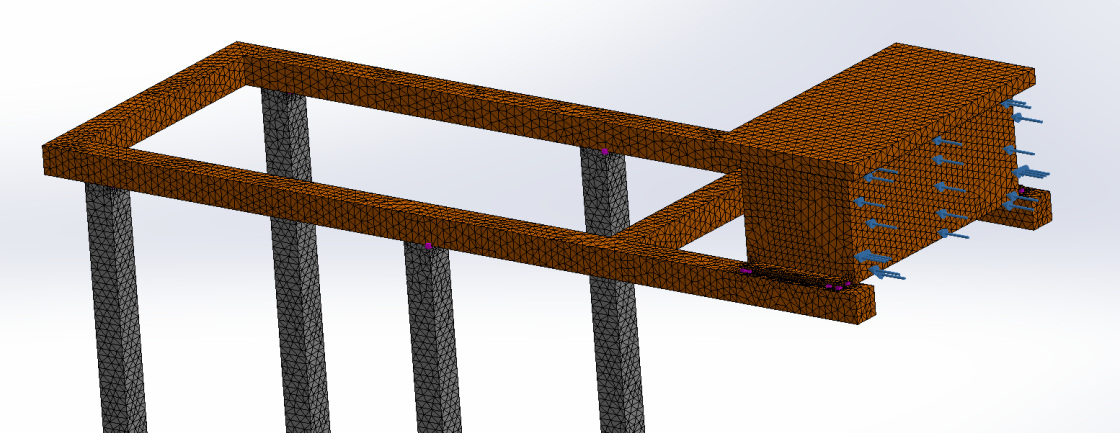

Figure 5.7. Pressure acting over top compartment.

5.4 Simulation

Before running the simulation, a couple of parameters must be set up first. The first one is to choose the material for the structure's elements, this simulation uses Aluminum alloy 6061 which has an elasticity modulus of 10,000 Ksi. Finally, the supports need to be set up. For this simulation, there are only four supports, one for each "leg" that supports the top frame and those supports are acting as fixed supports. Their movement is restricted in all directions. It is worth mentioning that the only important reaction forces are the ones on the X and Z direction. The reason for this is the cart can move on the Y axis, so if extreme loads are applied on the Y direction the cart will just move instead of deforming. Once these parameters are specified on the software the simulation can run.

With this simulation, we notice that the stresses on the supports area were too big, between 30 and 14 psi and did not correspond to the one calculated analytically (Figure 5.9). Analyzing the results, we concluded these stresses were affected because of the positioning of the supports. To

overcome this problem, we deleted the base of the structure and make small gaps on the frame itself to act as the supports. By doing this we eliminate the extra moment the length of the “legs” was creating.

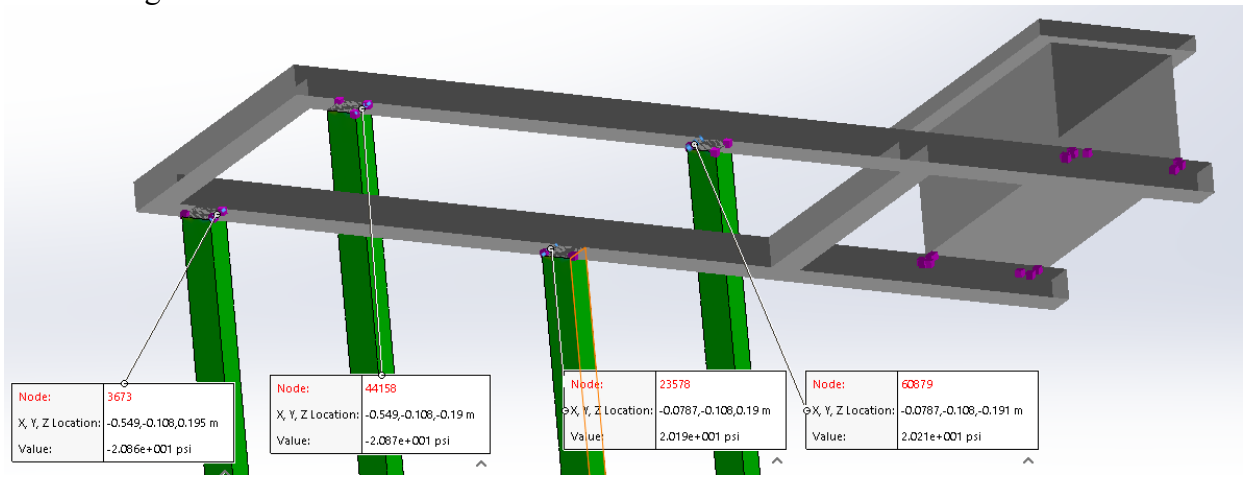

Figure 5.8. Results of first simulation.

After we changed the geometry of our body the whole process of preparation needed to be done again. For this we re-mesh the structure, selected the material, and set up the supports and the loads on the top compartment. Figure 5.10 shows the new geometry with its supports and the new mesh.

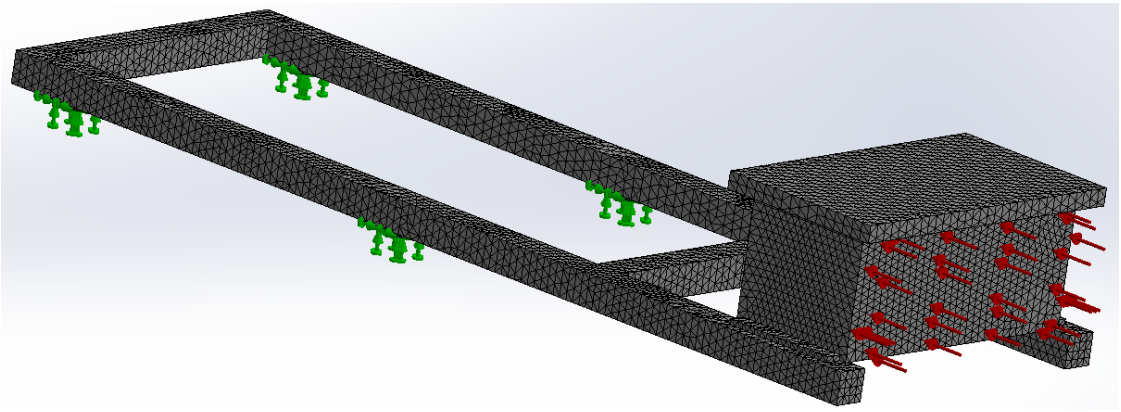

Figure 5.9 Final geometry with mesh, supports and loads.

The results if this new geometry were successful. It compares well to the solution acquired through the analytical method. Figure 5.11 show the results of this simulation, while table 5.1

compares the results of both analyses. As it was expected, the stresses on the Z direction are smaller on the simulation, this is because the different components of the top frame were joined to create one single body and was decided to dismiss its weight because it would create extra stresses due the excess of mass. This only affect the stresses on the Z direction but as it can be seen the distribution of the loads is very similar as the one estimated with the analytical method.

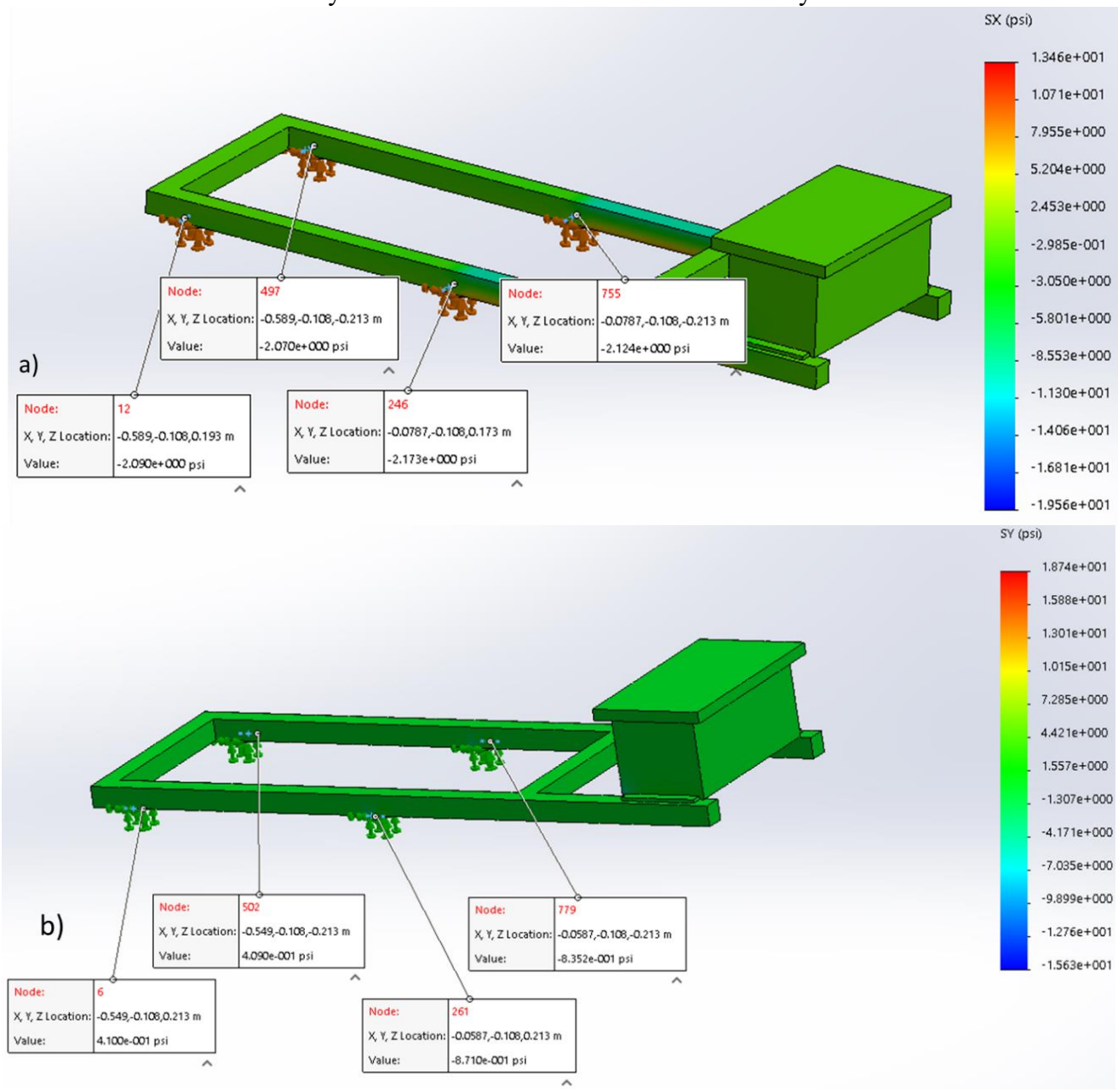

Figure 5.10 Results of simulation a) stress in X direction; b) stresses in Z direction.

Table 5.1 Results comparison.

	Analytical	Simulation	Difference
Unknowns	Force (lbf)	Force (lbf)	%
fai	0.74175	0.8476	12 %
fak	-7.4257	-0.3238	n/a
fbi	0.74175	0.8164	9.14%
fbk	4.42572	0.1524	n/a
fci	0.74175	0.8281	10.42%
fck	-7.4257	-0.3104	n/a
fdi	0.74175	0.8085	8.25%
fdk	4.42572	0.1520	n/a

Chapter 6: Results

6.1 Final Model

As mention in previous sections the main component of our tram cart is going to be aluminum fractional extrusions of one inch by inch and every part will be secure with button head socket cap screw grade 8 or higher of alloy steel with and T-nuts, both with a black phosphate finish to protected against corrosion (fig. x.1). Grade 8 bolts have a minimum tensile strength of 150,000 psi and a proof load of 120,000 psi. With these values we can calculate the screw's shear strength that is typically the sixty percent of the tensile strength, making it approximately 90,000 psi.

Figure 6.1. Screw and T-nuts used in joints.

The manufacturer provides several types of fastener application with their respective admissible forces. In this structure we are going to use joining strips (figure 6.2 a), corner brackets (figure 6.2 b) and corner gussets (figure 6.2 c). That supports direct forces of approximate 175, 325 and 325 lbs. and torsional forces of 400, 180 and 260 in/lbs.

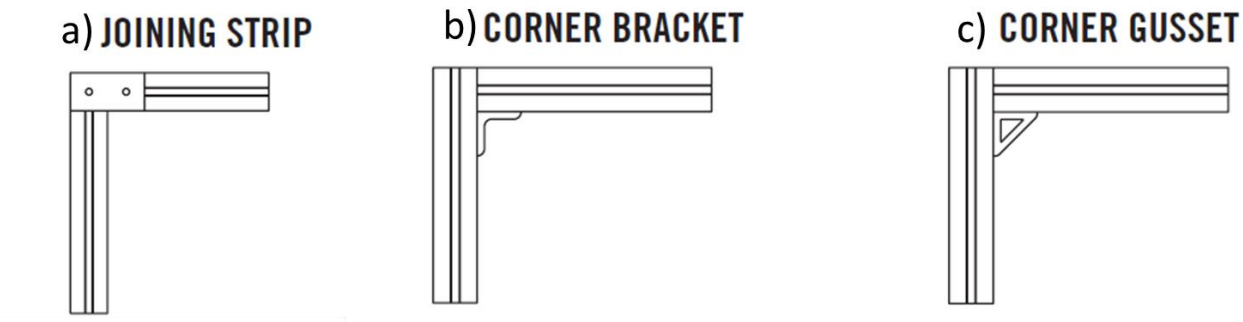

Figure 6.2 Fastener Applications.

The connectors where the only components missing from the model. Now that we have describe them and their properties we can discuss the final model. Figure 6.3 show the final design for the tram cart. As discussed previously the cart is mainly build of aluminum extrudes and has a height of approximately 1.2 meters and in extends 66 cm from the tracks for measuring. Table 6.1 shows a list of all the parts with their dimensions and part number for documentation purposes.

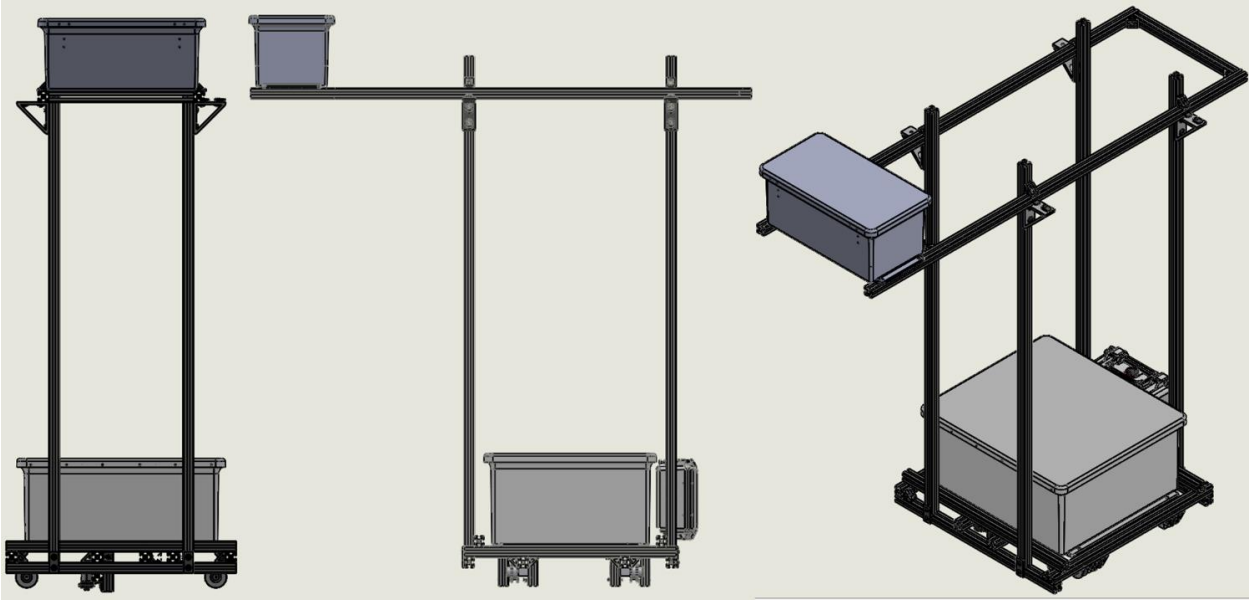

Figure 6.3. Tram cart's final design

Table 6.1 List of materials.

Part	Part No.	Description	Qty.	Location
Aluminum ext.	650000	1 x 1 x 52	2	Top frame
	650000	1 x 1 x 13.75	2	Top frame
	650000	1 x 1 x 47.24	4	Base
	650000	1 x 1 x 21.65	12	Base
	650000	1 x 1 x 3.75	4	Rollers
Connectors	653046	Joining Strip	6	Base
	653069	Corner Gusset	36	Top Frame
	653047	Corner Bracket	7	Base

	653073	Large Corner Gusset	4	Top Frame
	655371	45 degree supports	6	Base
Anti-detach	655222	Rollers	4	Base
	651119	90° Living nub	4	Base
Top compartment	J1407HPL	Stahlin enclosure	1	Top frame
Bot. compartment	J1816HL	Stahlin enclosure	1	Base
Control panel	1150	Pelican case	1	Base
Bolts	651169	1/4 20	100	Cart
T-nuts	651163	1/4 20	100	Cart

6.2 Final Loads and Results

With the specifications of the connections on the cart we can review the forces given by the analytical method to see if the materials were selected correctly or need to be replace. There are three critical areas that need to be inspect. The first one consists on the four supports for the top frame. For this analysis a system of equation was define on chapter 4 that help us calculate the resultant forces that the connectors will be under. The second part is where the four vertical bars connect with the base of the cart. And the last one is the rollers connected at the bottom of the cart that will prevent the cart from coming out of the tracks. For the first part the data obtain in chapter 4 will be use, for the third and second a new analysis like the one previously described will be performed and explained next.

Table 6.2 has the forces calculated in the previous chapter and its corresponding point can be seen on figure 6.4. The top frame is support by four long aluminum extrudes, these two parts are connected using eight corner gussets, two for each “leg”, one bellow the frame and one above (figure 6.4).

Table 6.2. Resultant forces for top frame part.

Points	Force (lb.)
Fa in x direction	0.74175
Fa in z direction	6.7477
Fb in x direction	0.74175
Fb in z direction	-3.7477
Fc in x direction	0.74175
Fc in z direction	6.7477
Fd in x direction	0.74175
Fd in z direction	-3.7477

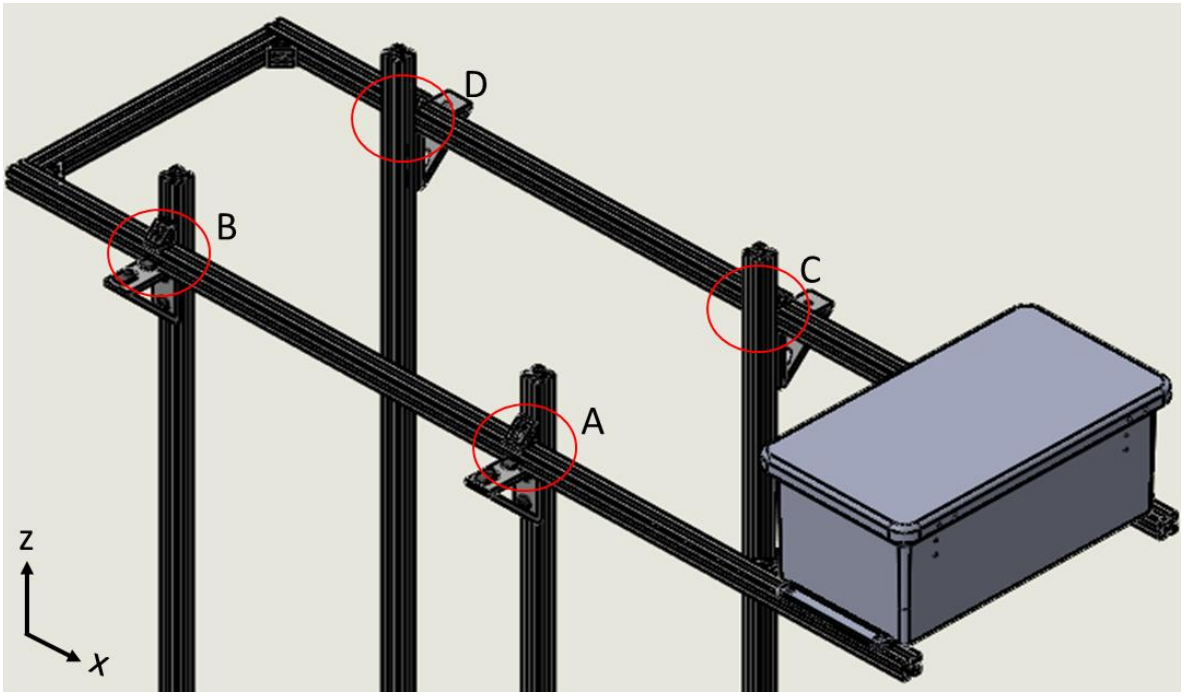

Figure 6.4. Points of interest on top frame.

Comparing the results of the analytical analysis with the specifications from the manufacturer for this type of connectors, which is up to 350 lbs. right above the support (figure 6.5), it can be said with confidence that it will work under the desire conditions.

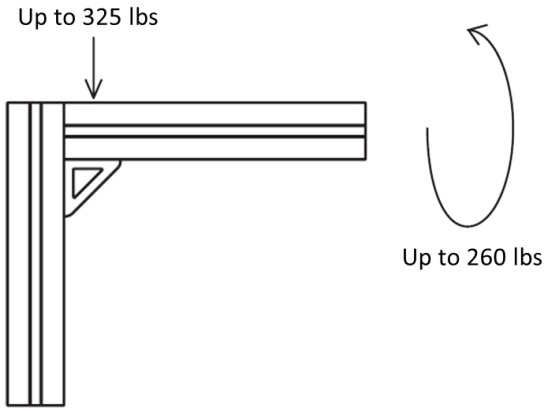

Figure 6.5 Manufacturer specification for corner gussets.

To start with the second analysis, we use a free body diagram to define all the forces acting on our system. This time instead of using the top compartment and the wind load as our main load, we used the resultant forces from the previous analysis in each point along with the wind loads affecting the bars and their weights. Figure 6.6 shows the free body diagram with all the forces that were considered with their magnitude and direction and the dimensions required for the analysis.

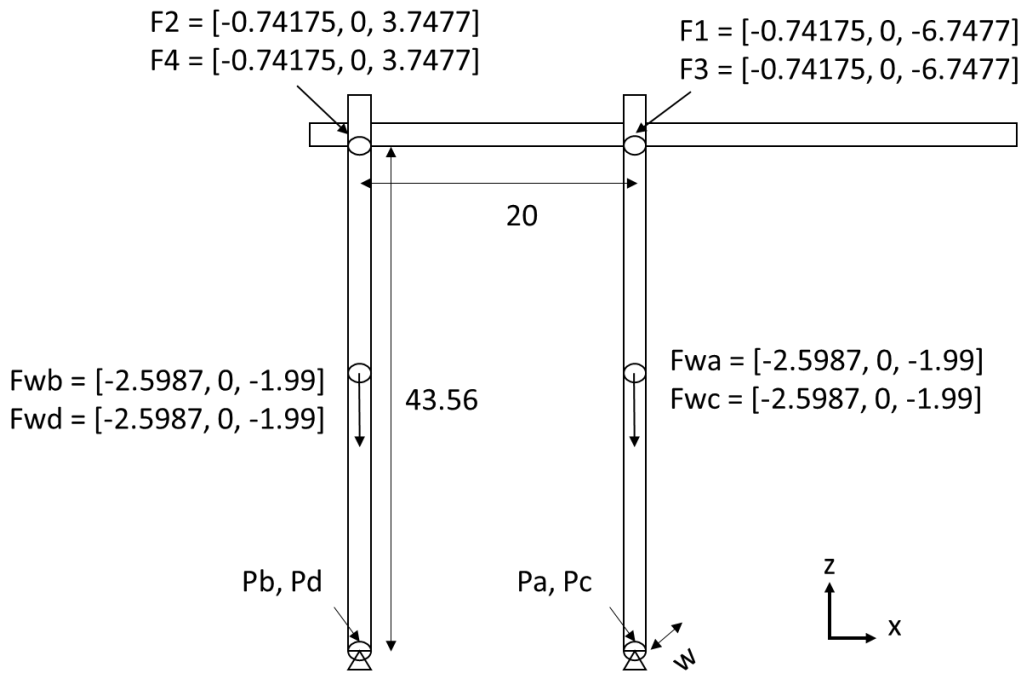

Figure 6.6. FBD of the second structure.

Table 6.2 Forces influencing second system.

Forces Coordinates	Forces
Pa = [20 0 0]	Fa = [fai faj fak]
Pb = [0 0 0]	Fb = [fbi fbj fbk]
Pc = [20 12 0]	Fc = [fci fcj fck]
Pd = [0 12 0]	Fd = [fdi fdj fdk]
P1 = [20 0 43.563]	F1 = [-0.74175 0 -6.7477]
P2 = [0 0 43.563]	F2 = [-0.74175 0 3.7477]
P3 = [20 12 43.563]	F3 = [-0.74175 0 -6.7477]
P4 = [0 12 43.563]	F4 = [-0.74175 0 3.7477]
Pwa = [20 0 21.7815]	Fwa = [-2.5987 0 -1.99]
Pwb = [0 0 21.7815]	Fwb = [-2.5987 0 -1.99]
Pwc = [20 12 21.7815]	Fwc = [-2.5987 0 -1.99]
Pwd = [0 12 21.7815]	Fwd = [-2.5987 0 -1.99]

For this analysis the point of origin selected was Pb and taking that as reference table 6.3 shows the rest of the forces coordinates and their magnitudes and directions. Following the same nomenclature as before, the unknowns are Fa, Fb, Fc, Fd and their components in x, y, z direction. And continuing the analysis we end it up with 12 unknowns and 6 equations.

```
% Moments
Ma = cross(Pa,Fa);
Mb = cross(Pb,Fb);
Mc = cross(Pc,Fc);
Md = cross(Pd,Fd);
M1 = cross(P1,F1);
M2 = cross(P2,F2);
M3 = cross(P3,F3);
M4 = cross(P4,F4);
Mwa = cross(Pwa,Fwa);
Mwb = cross(Pwb,Fwb);
Mwc = cross(Pwc,Fwc);
Mwd = cross(Pwd,Fwd);


% Forces and Moments Eq.
Feqn = Fa + Fb + Fc + Fd + F1 + F2 + F3 + F4 + Fwa + Fwb + Fwc + Fwd - 0;
Meqn = Ma + Mb + Mc + Md + M1 + M2 + M3 + M4 + Mwa + Mwb + Mwc + Mwd - 0;

% Eqn. Matrix
eqns = [Feqn(1) == 0    Feqn(2) == 0
        Feqn(3) == 0    Meqn(1) == 0
        Meqn(2) == 0    Meqn(3) == 0];
```

To be able to solve this equation system more equations are needed, as in the previous analysis we made used of the string equations (Hooke's law) and take the bars as rigid bodies, these assumptions gave enough equations and unknowns to solve the system. Table 6.3 and 6.4 show the equations the spring equations and the rigid body equation used to solve the problem.

Table 6.3 Spring equations

fak = kz * za	faj = ky * ya	fai = kx * xa
fbk = kz * zb	fbj = ky * yb	fbi = kx * xb
fck = kz * zc	fcj = ky * yc	fci = kx * xc
fdk = kz * zd	fdj = ky * yd	fdi = kx * xd

Table 6.4 Rigid Body Equations

xa = xb	xc = xd – (dz * w)	xd = xb + (dz * w)
ya = yb + (dz * d)	yc = ya + (dz * d)	yd = yb
za = zb – (dy * d)	zc = zb – (dy * d)	zd = zb + (dx *w)

Table 6.5 show the resultant forces acquired through MATLAB. As expected the forces in the X direction increased, this can be attribute to the moment created for the distance between the forces applied and the supports. While the forces in Z direction increased in one direction and decreased in other, or as they are in opposite direction both magnitudes increased on the same direction which is expected due to the wind loads. Although the forces on the Z axle are not high is good to considered that most of them will be absorb by the base due to gravity when pointing downwards. All the legs are connected with corner gussets, but they all are also resting on the horizontal bars that make up the base.

Table 6.5. Resultant forces for second system.

Points	Force (lb.)
Fa in x direction	3.3404
Fa in z direction	-0.1538
Fb in x direction	3.3404
Fb in z direction	7.1338
Fc in x direction	3.3404
Fc in z direction	-0.1538
Fd in x direction	3.3404
Fd in z direction	7.1338

The resultant forces for this system are below the limits recommended by the manufacturer, this means the cart will perform correctly and will not be come apart while operating on windy days.

The last critical area contrary to the previous ones will not predict whether the cart will stay in one piece because of external forces, but it will predict if the anti-detach system will perform as expected or if it will fail and needs an upgrade.

As the previous analysis we start with the free body diagram of the system (figure 6.7), defining the loads, dimensions and supports of the system. For this analysis the loads present will be the wind loads for all the bars, the weights of the two compartments and of the whole aluminum structure. There are eight supports on the cart. Four are the rollers that make up the anti-detach system and the other four are the wheels.

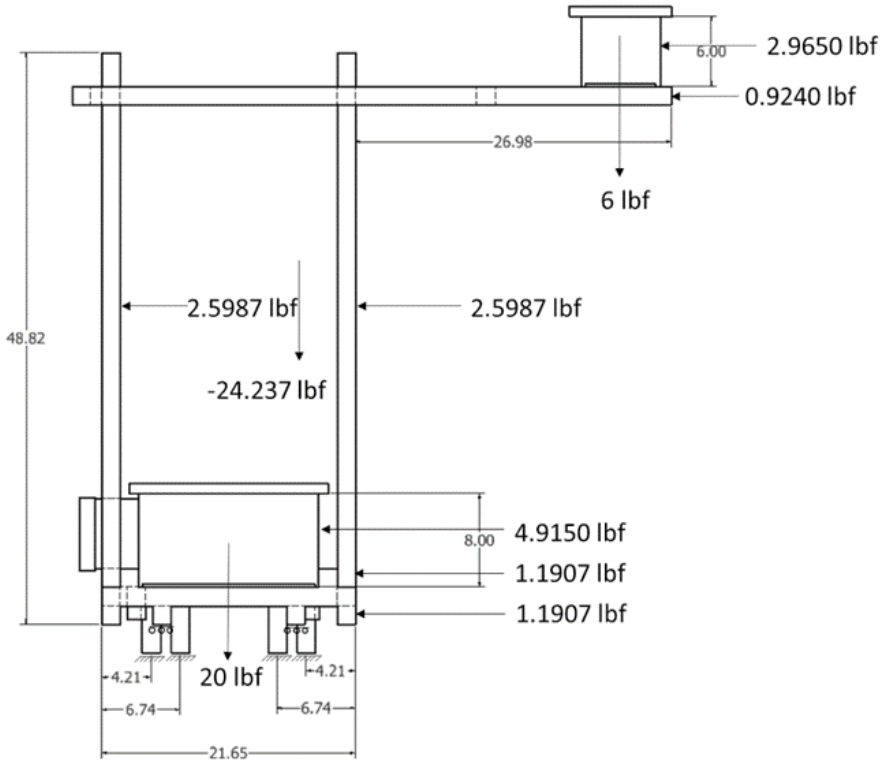

Figure 6.7. Tram cart's FBD

Before starting to solve the system, there are a couple of new consideration to take into account. The first one is for the loads, instead of defining the weight of each bar in its center of mass, the total weight of the structure (no enclosures) was calculated and positions as a single load at the center of mass of the it. The other considerations are for the supports. As mentioned before we are not considering forces in the Y directions, this is because the cart is going to be moving across that axis and because of this the resultant forces for the supports will not include this component. As for the wheels, they act as rollers, constraining movement in only one direction, in this case Z direction.

For this system we have 18 points of interest. P1-P4 are the supports for the anti-detach component starting from the far left, then P5-P8 are the wheels, starting with the far right in front of the previous supports then left front, the right back and finally left back. Pw1 and Pw2 are the top and bottom compartment while Pw3-Pw9 are the center of mas of the bars and Pw10 is the center of mass of the structure. Table 6.6 shows all the points of interest and theirs forces components.

Table 6.6 Forces influencing tram cart.

Forces Coordinates	Forces
P1 = [0 0 0]	F1 = [f1i 0 f1k]
P2 = [2.53 0 0]	F2 = [f2i 0 f2k]
P3 = [10.7 0 0]	F3 = [f3i 0 f3k]
P4 = [13.23 0 0]	F4 = [f4i 0 f4k]
P5 = [11.965 -4.012 2.816]	F5 = [0 0 f5k]
P6 = [1.265 -4.012 2.816]	F6 = [0 0 f6k]
P7 = [11.965 10.616 2.816]	F7 = [0 0 f7k]
P8 = [1.265 10.616 2.816]	F8 = [0 0 f8k]
Pw1 = [40.064 3.302 51.35]	Fw1 = [- 2.9657 0 -6]
Pw2 = [6.615 3.302 9.575]	Fw2 = [- 4.9150 0 -20]

Pw3 = [17.440 -2.7365 27.62]	Fw3 = [- 2.5987 0 0]
Pw4 = [17.440 9.3405 27.62]	Fw4 = [- 2.5987 0 0]
Pw5 = [-2.635 -2.7365 27.62]	Fw5 = [- 2.5987 0 0]
Pw6 = [-2.635 9.3405 27.62]	Fw6 = [- 2.5987 0 0]
Pw7 = [15.865 3.302 6.363]	Fw7 = [- 1.1907 0 0]
Pw8 = [15.865 3.302 3.2125]	Fw8 = [- 1.1907 0 0]
Pw9 = [43.439 3.302 47.563]	Fw9 = [- 0.9240 0 0]
Pw10 = [9.192 3.302 23.085]	Fw10 = [0 0 -24.437]

Although this time we have more points of interest, thanks to the considerations explained previously on the supports we end it up with twelve unknowns just as the previous analysis but start with four equations from moments and forces summations.

```
% Moments
M1 = cross(P1,F1);
M2 = cross(P2,F2);
M3 = cross(P3,F3);
M4 = cross(P4,F4);
M5 = cross(P5,F5);
M6 = cross(P6,F6);
M7 = cross(P7,F7);
M8 = cross(P8,F8);
Mw1 = cross(Pw1,Fw1);
Mw2 = cross(Pw2,Fw2);
Mw3 = cross(Pw3,Fw3);
Mw4 = cross(Pw4,Fw4);
Mw5 = cross(Pw5,Fw5);
Mw6 = cross(Pw6,Fw6);
Mw7 = cross(Pw7,Fw7);
Mw8 = cross(Pw8,Fw8);
Mw9 = cross(Pw9,Fw9);
Mw10 = cross(Pw10,Fw10);

% Forces and Moments Eq.
Feqn = F1 + F2 + F3 + F4 + F5 + F6 + F7 + F8 + Fw1 + Fw2 + Fw3 + Fw4 + Fw5 + Fw6 + Fw7 + Fw8 + Fw9 + Fw10- 0;
Meqn = M1 + M2 + M3 + M4 + M5 + M6 + M7 + M8 + Mw1 + Mw2 + Mw3 + Mw4 + Mw5 + Mw6 + Mw7 + Mw8 + Mw9 + Mw10 - 0;

% Eqn. Matrix
eqns = [Feqn(1) == 0   Feqn(3) == 0
        Meqn(1) == 0    Meqn(2) == 0];
```

To get more equations to solve the system we resort to the spring equations as in previous analysis, only this time we finish with 16 equations and 24 unknowns (table 6.7)

Table 6.7 Tram cart's spring equations

f1i = kx * x1	f1k = kz * z1	F5k = kz * z5
F2i = kx * x2	F2k = kz * z2	F6k = kz * z6
F3i = kx * x3	F3k = kz * z3	F7k = kz * z7
F4i = kx * x4	F4k = kz * z4	F8k = kz * z8

To complete the number of equations needed to solve the system of equations the rigid body equations are used. And as the previous equations these ones are different from the last two analyses. Table 6.8 shows the rigid body equation used for this analysis.

Table 6.8 Tram cart's rigid Body Equations

x2 = x1	z2 = z1 - (2.53 * dy)	z5 = z1 - (3.617*dx) - (11.965 * dy)
x3 = x2	z3 = z1 - (10.7 * dy)	z6 = z1 - (dy * 1.265) - (3.617 * dx)
x4 = x3	z4 = z1 - (13.23 * dy)	z7 = z1 + (10.761 * dx) - (11.965 * dy)
		z8 = z1 - (dy * 1.265) + (dx * 10.761)

Table 6.9 shows the resultant forces obtained using MATLAB and modifying the previous script to work with the new set of equations.

Table 6.9. Resultant forces for tram cart.

Forces Coordinates	**Forces**
P1 = [0 0 0]	F1 = [5.3952 0 13.4853]
P2 = [2.53 0 0]	F2 = [5.3952 0 10.4957]
P3 = [10.7 0 0]	F3 = [5.3952 0 0.8418]
P4 = [13.23 0 0]	F4 = [5.3952 0 -2.1476]
P5 = [11.965 -4.012 2.816]	F5 = [0 0 -1.9405]
P6 = [1.265 -4.012 2.816]	F6 = [0 0 10.7029]

P7 = [11.965 10.616 2.816]	F7 = [0 0 3.1779]
P8 = [1.265 10.616 2.816]	F8 = [0 0 15.8214]

The rollers used on the anti-detach system supports up to 50 lbs. according to the manufacturer specifications. Comparing this limit with the results obtain from the analysis, it is clear that the system will keep the cart on track with winds of 20 meters per second.

Reviewing the resultant forces from this analysis we can observe that the distribution of forces isn't even on the four wheels, this is because the anti-detach system is offset from the center to the left (figure 6.8 a). To get an even force distribution the rollers need to be shift to the center of the cart (figure 6.8 b). this will help to prevent one wheel wearing more than the others and give more stability and time of live to the whole system. Table 6.10 show the resultant forces for this case.

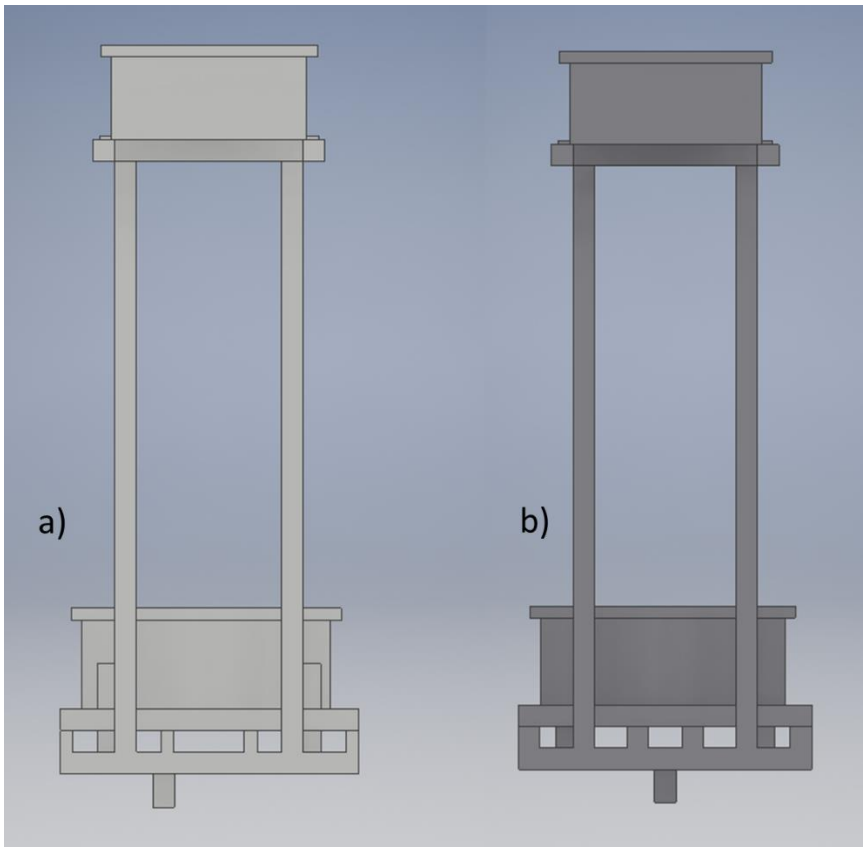

Figure 6.8 a) cart with offset supports; b) cart with centered supports.

Table 6.9. Resultant forces for tram cart with centered supports.

Forces Coordinates	Forces
P1 = [0 0 0]	F1 = [5.3952 0 14.1211]
P2 = [2.53 0 0]	F2 = [5.3952 0 11.1315]
P3 = [10.7 0 0]	F3 = [5.3952 0 1.4776]
P4 = [13.23 0 0]	F4 = [5.3952 0 -1.5118]
P5 = [11.965 -7.314 2.816]	F5 = [0 0 -0.0171]
P6 = [1.265 -7.314 2.816]	F6 = [0 0 12.6263]
P7 = [11.965 7.314 2.816]	F7 = [0 0 -0.0171]
P8 = [1.265 7.314 2.816]	F8 = [0 0 12.6263]

Lastly the same analysis was done but this time with the wind coming from the opposite direction. Figure 6.9 show the free body diagram used in these calculations.

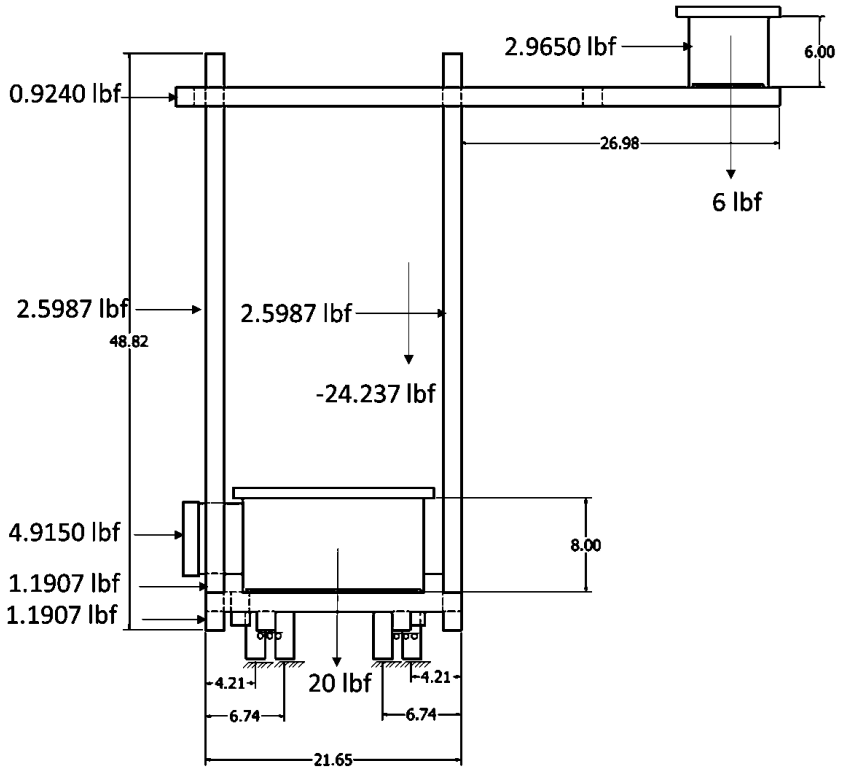

Figure 6.9 Tram Cart FBD, winds opposite direction.

As the wind loads are coming from the opposite direction, the surfaces in contact are going to be others and when converted to point loads its coordinates are going to change. Table 6.10 show the point forces coordinates and its components.

Table 6.10 Forces influencing tram cart.

Forces Coordinates	Forces
P1 = [0 0 0]	F1 = [f1i 0 f1k]
P2 = [2.53 0 0]	F2 = [f2i 0 f2k]
P3 = [10.7 0 0]	F3 = [f3i 0 f3k]
P4 = [13.23 0 0]	F4 = [f4i 0 f4k]
P5 = [11.965 -4.012 2.816]	F5 = [0 0 f5k]
P6 = [1.265 -4.012 2.816]	F6 = [0 0 f6k]
P7 = [11.965 10.616 2.816]	F7 = [0 0 f7k]
P8 = [1.265 10.616 2.816]	F8 = [0 0 f8k]
Pw1 = [35.689 3.302 51.35]	Fw1 = [2.9657 0 -6]
Pw2 = [- 2.1955 3.302 9.575]	Fw2 = [4.9150 0 -20]
Pw3 = [17.440 -2.7365 27.62]	Fw3 = [2.5987 0 0]
Pw4 = [17.440 9.3405 27.62]	Fw4 = [2.5987 0 0]
Pw5 = [- 2.635 -2.7365 27.62]	Fw5 = [2.5987 0 0]
Pw6 = [- 2.635 9.3405 27.62]	Fw6 = [2.5987 0 0]
Pw7 = [- 4.21 3.302 6.363]	Fw7 = [1.1907 0 0]
Pw8 = [- 4.21 3.302 3.2125]	Fw8 = [1.1907 0 0]
Pw9 = [- 6.675 3.302 47.563]	Fw9 = [0.9240 0 0]
Pw10 = [9.192 3.302 23.085]	Fw10 = [0 0 -24.437]

Using the same system of equation used on the previous analysis, (summation of moments and forces, spring and rigid body equations) the resultant forces on the system supports where calculated (table 6.11).

Table 6.11 Resultant forces on tram cart supports.

Forces Coordinates	**Forces**
P1 = [0 0 0]	F1 = [5.3952 0 11.2778]
P2 = [2.53 0 0]	F2 = [5.3952 0 -4.7963]
P3 = [10.7 0 0]	F3 = [5.3952 0 16.1339]
P4 = [13.23 0 0]	F4 = [5.3952 0 22.6154]
P5 = [11.965 -7.314 2.816]	F5 = [0 0 18.0870]
P6 = [1.265 -7.314 2.816]	F6 = [0 0 -9.3247]
P7 = [11.965 7.314 2.816]	F7 = [0 0 23.2055]
P8 = [1.265 7.314 2.816]	F8 = [0 0 -4.2061]

Applying the same support distribution to distribute loads equitably shown in figure 6.8 b, the resultant forces change as shown on table 6.12.

Table 6.12 Resultant forces on tram cart centered supports.

Forces Coordinates	**Forces**
P1 = [0 0 0]	F1 = [5.3952 0 -10.6419]
P2 = [2.53 0 0]	F2 = [5.3952 0 -4.1605]
P3 = [10.7 0 0]	F3 = [5.3952 0 16.7697]
P4 = [13.23 0 0]	F4 = [5.3952 0 23.2512]
P5 = [11.965 -7.314 2.816]	F5 = [0 0 20.0105]
P6 = [1.265 -7.314 2.816]	F6 = [0 0 -7.4012]
P7 = [11.965 7.314 2.816]	F7 = [0 0 20.0105]
P8 = [1.265 7.314 2.816]	F8 = [0 0 -7.4012]

Chapter 7: Conclusions

7.1 Summary

"Mid-range" sensing systems have been used in RSE for a while, and have proof to be useful, providing mapping from specific areas with greater detail that using conventional methods and sometimes measuring areas not available through these methods. Even though the systems have different modes of operating (manual, semi-automatic, automatic) its design and specifications do not allow them to be leave on site to act remotely and withstand the weather conditions without leaving the expensive equipment inside of them unprotected.

In this work, a "mid-range" sensing system is reviewed to see his functionality, and its areas of improvement to be use on the field with minimum human interaction and based in this propose a new system that will be able to perform remotely and withstand the field conditions. This work started with several visits to the facility where the cart will be operation, this to be in direct contact with the environment where it will be performing and to review the current state of the system and the actions needed to make the system operational. After reviewing the current system this were the observations.

- No weather protection
- More stiffness needed
- No remote connectivity
- Lack of automated simultaneous sensing

To address those issues a new system was designed, using mainly 6560 aluminum alloy extrusions for the body of the cart, protecting in against corrosion. Two special enclosures were implemented to protect all the electronics and the rest of the equipment. These compartments have a level of protection similar to a IP66 certification and are manufactured to be in exterior for prolongated times. After that, the distribution of the electronics was defined, and a special electronic board was created to achieve the simultaneous sensing onboard. And finally, to finish with the design a docking station and an anti-detach system were added to the design so it can charge itself after each cycle and stay on track even with strong winds.

Once the new cart was design a structural analysis was performed on the new structure, considering weights, wind loads and supports. The overall analysis consisted in three analyses for each area of interest. The first one was the top frame. This one helped predict if the overhang sensors will be safe and that the bars will support their weights along with the wind loads. The second one was to determine the structure integrity, it concentrated on the 4 vertical bars that hold the top frame in place, for this one the forces calculated on the first analysis were used along the wind loads to see how the support will respond. And the final one focused on the more important part, the anti-detach mechanism. These calculations include the weights of every component and the loads produce due to strong winds hitting the bars.

All the analysis gave positive results, proving that this new design will be performing with no problem regardless the weather conditions. As long as they don't surpass the ones stated on this work. As a general measure in this analysis all the supports have safety factor above 2.0 which for structure that are not in constant interaction with human life is a good standard.

7.2 Research Contributions

Many researchers have been using mid-range sensing systems successfully for a while. Whether it uses a tram cart, cable way, UAS or kites most systems are not permanently positioned to be "ready-to-sense" whenever the user needs to. This work solves this problem by providing an analytical proven tram cart design that will perform constantly on the Jornada Experimental Ranch regardless the season or weather. The main contributions of this work are as follows:

- Structural analysis to simulate loads affecting the system and predict fails on their components.
- Material selection for system to withstand average weather condition on JER.
- Improvement of measurement (quantitative and qualitative).
- Improve productivity of research work by eliminating extra tasks for research teams (assemble and preparation of the unit).
- Improve availability of the cart.

7.3 Future Work

One of the main functions of the Systems Ecology Lab is to examine and model changes in plant and ecosystems over time. This work completes the hardware design for a new mid-range sensing system, along with the software written by previous students this unit is ready for build. The next step in the development of this unit is to update the software controlling the sensors to work with the new mechanisms, board and sensors. Once this is done the cart will be ready to test and collect data which will be use by the researcher to visualize and analyze the changes on the vegetation of the site in Jornada Experimental Range.

References

[1] Rees, W. G. (2001). Physical Principles of Remote sensing (Second ed.). Cambridge, United Kingdom: Cambridge University Press.

[2] Sabins, F. F. (2000). Remote sensing: Principles and interpretation (Third ed.). New York: W.H. Freeman and Co.

[3] Randall, B. S. (2012). Introduction to Remote Sensing of Environment (RSE). MicroImages Inc.

[4] Gamon, J. A., & Cheng Y. (2006). A mobile tram system for systematic sampling of ecosystem optical properties, Remote Sensing of Environment, 103, 246-254.

[5] Moncreiff, J. B., Malhi, Y., & Leuning, R. (1996). The propagation of errors in long-term measurements of land-atmosphere fluxes of carbon and water. Global Change Biology, 2, 231-240.

[6] Leffler, A.J., Hollister, R., Tweedie, C. E., & Vargas, S.A. (2014). A Mobile Instrumented Sensor Platform for Long-Term Terrestrial Ecosystem Analysis: An Example Application in an Arctic Tundra Ecosystem. Journal of Environmental Informatics, 24, 1-10.

[7] Systems Ecology Lab. (n.d.). Retrieved January 27, 2018, from https://sel.utep.edu/

[8] Weather Gauges on the Jornada. (n.d.). Retrieved November 23, 2018, from https://jornada.nmsu.edu/data-catalogs/weather-gauges

[9] GCSE Geography - Hot deserts. (n.d.). Retrieved November 23, 2018, from http://www.bbc.co.uk/schools/gcsebitesize/geography/ecosystems/desert_rev1.shtml

[10] Degrees of Protection Provided by Enclosures (IP Code), ANSI/IEC § 60529 (2004).

[11] Ochoa, E., M.S. (n.d.). Robotic Tram Line for Field Data Collection [Scholarly project].

[12] Hibbeler, R. C. (2012). Structural Analysis (Eighth ed.). New Jersey: Pearson Prentice Hall.

[13] Budynas, R.G., & Nisbett, J. K. (2011). Shigley's Mechanical Engineering Design (Ninth ed.). New York: McGraw-Hill.

Vita

Quetzalcoatl Mendoza Rosas was born in Lazaro Cardenas, Michoacan, Mexico. The second son of Rafael and Rosy, he graduated from Universidad De La Salle Bajio High School, Leon, Guanajuato, Mexico, in spring of 2010. He was accepted into the Instituto Tecnologico de Celaya in the summer of 2010 to start his bachelor's in engineering. After earning his bachelor's degree in mechatronics engineering in fall 2015 he moved to El Paso, Texas for an internship at a steel mill factory, and stayed to join graduate school at the University of Texas at El Paso. In spring 2016 joined the System Ecology Lab as research assistant working under Dr. Craig Tweedie and M.S. Gesuri Ramirez to develop electronic boards and embedded software for environmental data acquisition on the artic and the desert.

Contact Information: qmendozaro@miners.utep.edu

This thesis was typed by: Quetzalcoatl Mendoza Rosas.